

J. A. Gray, P. J. Donatelli, P. M. Yavorsky

U.S. Energy Research and Development Administration  
Pittsburgh Energy Research Center  
4800 Forbes Avenue  
Pittsburgh, Pennsylvania 15213

#### INTRODUCTION

Of the many processes currently under development which will convert coal to environmentally acceptable solid, liquid, and gaseous fuels utilizing pyrolysis, synthesis gas, solvent extraction, or hydrogenation techniques, the direct hydrogenation of coal to a raw gas that is easily upgraded to pipeline quality is a promising approach. Such a process is under development by the E.R.D.A., Pittsburgh Energy Research Center and is known as HYDRANE (1, 2).

Briefly, the HYDRANE flow sheet is as follows. Pulverized raw coal is fed to the top zone of the hydrogasifier, operated at 70 atm and 750°-900° C, where it falls freely as a dilute cloud of particles through a hydrogen-rich gas containing some methane from the lower zone. About 20 pct of the carbon in the raw coal is converted to methane, causing the coal particles to lose their volatile matter and agglomerating characteristics and to form very porous, reactive char particles. This char falls into the lower zone, operated at 70 atm and 900°-980° C, where hydrogen feed gas maintains the particles in a fluidized state and reacts with an additional 25 pct of the carbon to make methane. The product gas exists from the bottom of the dilute-phase zone and is cleaned of entrained solids, tars and oils, and some unwanted gases. After cleanup, catalytic methanation of the small amount of residual carbon monoxide gives a pipeline quality, high-Btu, substitute natural gas. Char from the lower zone of the hydrogasifier is reacted with steam and oxygen to make the needed hydrogen.

This process has the following advantages:

1. External hydrogen consumption per unit of methane produced is low because the hydrogen already in the coal is efficiently utilized,
2. Process costs associated with coal pretreatment, inherent in other coal conversion processes based on caking bituminous coal feedstocks, are eliminated,
3. 95 percent of the product methane is produced directly in the hydrogasifier thus requiring very little catalytic methanation,
4. Simple reactor design,
5. Produces low-sulfur char byproduct for hydrogen generation and low-sulfur tars, and
6. Utilizes sensible heat of the residual char from the hydrogasifier in the hydrogen generation plant.

Because of these advantages, coal and oxygen (the costliest items in gasification) requirements are minimized for the process, and thermal efficiency and carbon utilization are high at 78 pct and 44 pct, respectively (3, 4).

Much of the hydrogasification kinetic data on the laboratory scale, free-fall, dilute-phase reactor has already been published (5, 6) as well as data from a semiflow bench-scale reactor (7). In this paper we review previous and some recent kinetic data with regard to the type of reactor used to obtain the data, and the effect of the type of reactor on the conversion data. The conversion of the non-mineral elements in the coal during hydrogasification and the char yield are shown to be related to the carbon conversion regardless of the reactor geometry used, so that the constituent conversions can be calculated once the carbon conversion is known. This simplifies the reactor design in that only the carbon conversion need be kinetically defined for a particular reactor geometry.

#### EXPERIMENTAL REACTORS

##### "Hot-Rod" Reactors (HR)

In 1955 El Paso Natural Gas Company entered into a cooperative agreement with the then U.S. Bureau of Mines Synthetic Fuels Research Branch to investigate the hydrogenation of a subbituminous New Mexico coal to produce high-Btu gas and low-boiling aromatics. Part of the agreement called for tests in a reactor in which dry coal could be rapidly brought to the desired operating temperature and pressure. A normal autoclave required over an hour to reach temperature. Consequently, the effect of the heating and cooling cycles on the reaction could not be discerned. In late 1955, Hiteshue conceived the apparatus known as the "hot-rod" reactor and completed the El Paso project using it. The apparatus along with conversion data were first reported by Hiteshue, Anderson, and Schlesinger in 1957 (8) and again during 1960-1964 (9, 13).

The "hot-rod" reactor, shown in Figure 1, was a 70-inch long stainless steel tube (type 304) having a 5/16-inch inside diameter and a 5/8-inch outside diameter. A coal or char sample weighing 8 grams and screened to 30 x 60 U.S. sieve size was inserted into the tube between two porous stainless steel disks such that a 32-inch length was available to fluidize the sample. The tube was heated with electrical current by connecting it to a transformer that was capable of supplying 700 amperes at 9 volts. With this method of heating, the reactor, sample, and feed gas were heated from room temperature to 800° C in about 2 minutes and to 1200° C in about 4 minutes. At the end of the experiments, the reactor and sample were cooled to room temperature in about 10 seconds by spraying with cold water. The flowsheet of the entire apparatus is shown in Figure 2 and has been discussed in detail in the previously cited references.

##### Free-Fall Dilute Phase Reactor (FDP)

The agglomeration of bituminous coals in hydrogen is a major problem in designing a reactor for their continuous hydrogenation to produce a high-Btu gas. It has been shown that bituminous coals, both caking and noncaking, will agglomerate when rapidly heated in hydrogen at 500 psig and 500° C or at 6,000 psig and 500° to 800° C (10, 13, 14). Texas lignite agglomerated at 6,000 psig and 800° C but did not agglomerate at 500 psig and 500° C. Chars produced from carbonizing bituminous coals, cokes, graphite and anthracite, and a highly oxidized hvAb coal did not agglomerate. Feldmann (6) observed that at least 10 pct of the volatile matter in Pittsburgh seam hvAb coal, originally containing 36 pct volatile matter, had to be removed to obtain a char that would not agglomerate at 1,000 psig and 800° C in hydrogen in subsequent "hot-rod" reactor tests.

Lewis and Hiteshue (15) designed an entrained flow reactor for continuously hydrogenating both caking (hvAb) and noncaking (hvCb) coals. They believed that if the suspension of coal in the feed gas was dilute enough (dilute phase), particle-

particle collision and subsequent agglomeration could be avoided. The reactor was a 1/8-inch inside diameter, 60-foot long helical tube, and was operated at 600 psig and 800° C. The coal was entrained at a rate of 60 gms/hr in hydrogen where the hydrogen velocity was 2 fps. Experiments with the helical reactor were unsuccessful because of solids plugging at about the 500 to 550° C zone in the helical tube. Changing to a straight, horizontal tube reactor having an internal diameter of 5/16 inches and a length of 20 feet did not alleviate the plugging problem.

A 4-inch diameter vertical reactor where the coal particles would not contact the reactor wall during devolatilization was found to operate very successfully. It was further shown that reducing the diameter to less than 3 inches caused plugging, again due to coal particles contacting the reactor wall. Figure 3 shows the laboratory dilute-phase reactor that evolved from these studies.

A large amount of kinetic data has been reported for this reactor using Pittsburgh seam hvAb and Illinois #6 hvCb coals (5, 6, 16, 17). Details of the laboratory reactor and method of operation are discussed in the previous references.

The present FDP reactor is a 3.26-inch inside diameter pipe that is heated through the wall and contained in a 10-inch diameter pressure shell. Coal is injected into the top of the reactor through a 5/16-inch inside diameter, water-cooled nozzle using a rotary feeder and part of the feed gas. The coal free-falls through a 5-foot long reactor concurrently with the feed gas at a particle residence time of less than a second. Agglomeration is avoided because the rapid heating devolatilizes the particles before many particle collisions with the wall or other particles can occur. The char product is recovered from a cooled hopper after each experiment and is analyzed. Gas flows and compositions are measured over steady state periods of the experiment so that mass balances can be calculated.

#### Two-Stage Integrated Reactor

In order to react fresh dilute phase char with hydrogen as in the integrated reactor system described previously, and to measure reactivity and methane yield at carbon conversion levels expected in a commercial reactor, a two-stage laboratory hydrogasifier was built consisting of a dilute-phase reactor integrated with a second stage reactor that could be operated as either a moving-bed or fluid-bed reactor. Figure 4 illustrates the version using a fluid-bed second stage. Because the diameter of the coal particles increased substantially due to swelling and some agglomeration during devolatilization, a char crusher was used to reduce the particle size to a level acceptable for fluidization. In the moving-bed version, no crusher was used as shown in Figure 5.

The true composition of product gas from the individual stages could not be determined directly because a large amount of mixing occurred between gas near the bottom of the dilute phase reactor and gas near the top of the second stage reactor. The overall methane yield for the two-stage unit was determined in some cases, and these yields were compared to yields from previous dilute phase reactor experiments. The mixing problem was not unexpected since there was no gas seal leg used between the two reactors because of the small scale of the equipment. The mixing was caused from convection currents created from the falling char particles and the hot reactor walls. The operation of the two-stage hydrogasifier is described in much greater detail elsewhere (18).

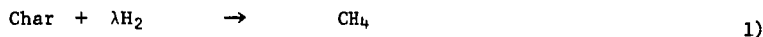
#### KINETIC MODEL

Within about the first few inches of free-fall in the FDP reactor, the coal particles are rapidly heated and devolatilized yielding a "popcorn" char (19). It is generally accepted that during the period of devolatilization, chemical bonds

such as methylene bridges, oxygen bonds, and side chains are easily broken resulting in evolution of hydrogen rich volatile matter and a large number of free radical structures (5, 20, 21, 22). These free radicals can react with hydrogen forming hydrocarbon gases and solid species that are active for further hydrogenation to volatile material or combine by polymerization to form a highly aromatic, unreactive char structure. During free-fall, but after rapid devolatilization has occurred (after about 6 inches), the solid carbon is very reactive in behavior as though not enough time has elapsed for significant polymerization to proceed (5). However, when the char is further reacted with hydrogen in a second-stage reactor such as a fluidized-bed or moving-bed, the hydrogasification rate is about two orders of magnitude slower (1, 18). Thus, the coal structure and reactivity change constantly during reaction.

Feldmann (5) has proposed that for kinetic modeling purposes the carbon in the raw coal can be divided into three types during hydrogasification. Type 1 carbon is the highly reactive species which is flashed off almost instantaneously during rapid heat-up and devolatilization, Type 2 is the solid carbon which readily hydrogasifies during most of the particle free-fall, and Type 3 is the low-reactivity carbon contained in the remaining, polymerized char structure. Johnson (23) has proposed a very similar model.

In developing a reaction rate expression for the hydrogasification of coal in the FDP reactor (5), the Type 1 carbon is assumed to devolatilize instantaneously and the remainder of hydrogasification occurs with Type 2 carbon. The reaction can be written as



for the data at high hydrogen partial pressures ( $P_{\text{H}_2}$  50-60 atm) (5), and as,



for data at lower hydrogen partial pressures (6). An empirical correlation of  $\lambda$ , the stoichiometric coefficient, has been developed from the high pressure data and is

$$\lambda = \begin{cases} 1.0 & \text{for } x < 0.45 \\ 8x - 2.6 & \text{for } 0.45 \leq x \leq 0.55 \\ 1.8 & \text{for } x > 0.55 \end{cases} \quad 3)$$

where  $x$  is the total fractional carbon conversion.

The oil yield has been as high as 5% for Pittsburgh seam hvAb coal and 6% for Illinois #6 hvCb coal. A small amount of carbon oxides are produced (usually less than 4% of the product gas) and are in equilibrium according to the water-gas shift reaction as shown in Figure 6.

The hydrogasification of Type 2 carbon follows the rate equation

$$\frac{dx}{dt} = k P_{\text{H}_2} (\alpha - x) \quad 4)$$

where  $x$  is the fractional carbon conversion,  $P_{\text{H}_2}$  the hydrogen partial pressure,  $\alpha$  the

fraction of the carbon which is available for reaction in the regime being considered and  $k$  the reaction rate constant. Another way of writing Equation 4 where the devolatilized carbon is not included in the fractional carbon conversion is

$$\frac{dZ}{dt} = k P_{H_2} (\beta - Z) \quad 5)$$

where  $Z = (x-E)/(1-E)$  and  $\beta = (\alpha-E)/(1-E)$ .  $E$  corresponds to the fraction of carbon that was devolatilized. Assuming the coal particles being fed to the dilute phase reactor attain terminal velocity and the same temperature as the reactor wall almost immediately, Equation 4 may be applied to the FDP reactor as

$$U_T \frac{dx}{dL} = k P_{H_2} (\alpha - x) \quad 6)$$

where  $U_T$  is the particle terminal velocity. Equation 6 is integrated over the reactor length yielding

$$\int_E^x \frac{dx}{\alpha - x} = k P_{H_2} \frac{L}{U_T} \quad 7)$$

In the integration,  $P_{H_2}$  is assumed constant and equal to the hydrogen partial pressure in the product gas because extensive backmixing occurs due to the hot reactor walls and the downward flow of char. The fraction of Type 1 carbon is accounted for as  $E$  in the integration. Within the constraint that  $0 < \alpha \leq 1$ , the best fit of carbon conversion data from the FDP reactor is obtained when  $\alpha = 1$  (2). This means that essentially all of the carbon is available for hydrogasification.

The hydrogasification of char in a "hot-rod", moving-bed, or fluid-bed reactor follows the same rate expression given by Equation 4, however, the reaction is much slower because most of the carbon that is reacting is of the Type 3 variety. Application of Equation 4 to fluid-bed and moving-bed reactors has been discussed elsewhere (18).

The rate expression does not take into account transitions between the various reactive types of carbon in the coal nor mass transfer resistance. In fact the hydrogasification of char is so complex because of the change in carbon structure during reaction, that the above simple classification of carbon may not apply in all cases. Johnson's model (23) takes into account the continuous deactivation of the char but also adds another constant into the model which must be evaluated using experimental data. Generally the more constants there are in a model, the better the model will fit regardless of the accuracy of the proposed reaction mechanism, and the more experimental data is needed to evaluate the constants. For this reason, Equation 4 was kept simple so that data from various reactors could be easily compared. With this perspective, the data from each of the reactor systems will now be discussed.

## EXPERIMENTAL RESULTS

### FDP Reactor

Using Equation 7 and a terminal velocity of 9 fps, Feldmann (5) determined  $E$  and  $k$  values for carbon conversion data at 900° C and 725° C. These values are listed in Table 1. In a later publication, Feldmann (2) reanalyzed the 725° C data as a function of hydrogen partial pressure and presented recent 850°-900° C (total

TABLE 1.- FDP Reactor kinetic data (5)

Reactor Wall Temp., °C	Total Reactor Press., atm	E, %	$k$ $\text{atm}^{-1}\text{hr}^{-1}$
725	103,205	22	6
900	205	14	21

TABLE 2.- Ultimate and proximate analyses of feeds

Run Series	Coals				Chars	
	HR-1	HR-2	FDP	HR-1C	HR-2C	
Wt. %	Pgh hvAb	Pgh hvAb	Pgh hvAb	Ill. #6 hvCb	Pgh hvAb	Ill. #6 hvCb
C	74.2	74.1	78.1	74.4	78.8	83.9
H	5.1	5.1	5.3	5.2	1.9	2.8
N	1.5	1.5	1.6	1.7	1.6	---
S	1.9	1.5	1.1	1.3	1.1	---
O	8.8	7.6	8.2	11.5	1.9	---
Ash	8.5	10.2	5.7	5.9	14.7	10.2
	100	100	100	100	100	---
Moisture	1.9	1.4	1.2	1.4	0	0.9
VM	33.9	35.3	36.4	36.8	---	26.0
FC	56.5	53.1	56.7	55.9	---	---

TABLE 3.- FDP Reactor kinetic data

Reactor Wall, Temp., °C	Total Reactor Press., atm	E, %	$k$ $\text{atm}^{-1}\text{hr}^{-1}$
725	103,205	23.1	5.3*
725	103,205	9.4	14.7
850-900	69-108	21.5	24.7*
850-900	69-108	12.2	33.0

\*Total carbon conversion.

pressure 69-108 atm) data (6). The ultimate and proximate analyses of the feed coals are shown in Table 2 for the FDP and "hot-rod" reactors. Figures 7 and 8 show the carbon conversion data as total carbon conversion and as carbon conversion to equivalent methane (carbon in methane and ethane).

The difference between total carbon conversion and carbon conversion to methane is due mainly to the production of carbon oxides and oil. Some experimental error is also introduced in measuring the flowrate and composition of the feed and product gases, and in recovery and analysis of the solid and liquid products. Often the run times were not long enough to collect enough oil so the yield could be accurately measured (2). These errors become obvious when the carbon and ash recoveries are much lower than 100 pct. Figure 9 indicates that the hydrogen partial pressure as well as reactor temperature greatly influences the amount of oil produced, especially below a partial pressure of 30 atm. The increase in oil yield with decreasing hydrogen partial pressure agrees with the divergence of the two carbon conversion curves in Figures 7 and 8. Apparently the higher hydrogen partial pressures enhance the hydrocracking of the oil products. Residence time of the hydrocarbon vapors in the reactor also affects the oil yield causing lower amounts of oil at increasing residence time as shown in Figure 10. As indicated in Figure 5, the oil yield was determined by recovery from the gas sample and main tail gas streams. However, some of the oil was lost by condensation on the char receiver wall and to some extent on the char in the receiver. Therefore the oil yield data are now being reexamined where the yield in the gas sample stream is multiplied by the ratio of the total product gas flowrate to the sample gas flowrate in order to estimate total oil yield. These values will probably be higher than the reported values.

The values of the kinetic parameters in Equation 7 for the data in Figures 7 and 8 are listed in Table 3. These parameters were evaluated both for total conversion and for carbon conversion to equivalent methane. The value of  $\alpha = 1$  gave the best fit of the total carbon conversion data and was subsequently used to fit the carbon conversion to methane data. The terminal velocity of a single char particle was calculated using the equation

$$U_T = \left[ \frac{3.1g(\rho_s - \rho_g)\bar{d}_p}{\rho_g} \right]^{1/2} \quad 8)$$

for  $500 < Re_p = \frac{\bar{d}_p U_T}{\nu_g} < 200,000$  (24), and correcting this value for the effect of the cloud of particles (25). Table 4 lists the parameters used for calculating the terminal velocities. A terminal velocity of 16.5 fps was used for the 850°-900° C data and 10.7 fps (average of 9.9 and 11.5) for the 725° C data.

The total reactor pressure has a large influence on the terminal particle velocity because the pressure determines for the most part the size of the char particles produced and hence the bulk and particle densities. This is illustrated in Figure 11 where the char bulk density is plotted versus total reactor pressure. As the pressure increases, the bulk density increases. The bulk density is higher when the feed gas contains about 50 pct methane instead of pure hydrogen. Apparently, increasing the reactor pressure dampens the explosive emission of gases during the rapid devolatilization reaction. A high concentration of hydrogen in the reactor causes more of the carbon to be reacted out of the particle structure resulting in a lower bulk density char (and lower particle density) than is obtained when the reactor feed gas contains about 50 pct methane. Some char particle size data is listed in Table 5 showing how increases in reactor temperature and pressure cause decreases in the mean char particle diameter.

TABLE 4.- Parameters used to calculate terminal velocity

Temperature, ° C	725	725	900	900
Pressure, atm	205	103	205	69
W, lb/hr ft <sup>2</sup>	165	128	145	207
d <sub>p</sub> , in.	0.0521	0.0667	0.0345	0.0660
ρ <sub>b</sub> , lb/ft <sup>3</sup>	13.33	8.0	12.29	5.8
ρ <sub>s</sub> <sup>*</sup> , lb/ft <sup>3</sup>	36.8	22.1	33.9	16.0
ρ <sub>g</sub> , lb/ft <sup>3</sup>	1.408	0.7074	1.199	0.4035
μ <sub>g</sub> , lb/ft hr	0.05745	0.05745	0.06409	0.06409
U <sub>TS</sub> , fps	3.3	4.1	2.8	4.6
Re <sub>p</sub>	1264	1010	542	573
U <sub>T</sub> /U <sub>TS</sub> <sup>**</sup>	3.0	2.8	3.0	3.6
U <sub>T</sub> , fps	9.9	11.5	8.4	16.5

\* Estimated by the ratio of bulk densities and particle density of 16.0 lb/ft<sup>3</sup> (26) for char produced at 850°-900° C and 69 atm, e.g.,  $\frac{13.33}{5.8} \times 16 = 36.8$ .

\*\*Ratio of terminal velocity to single particle terminal velocity at a specific mass feed rate per unit area (25).

TABLE 5.- Effect of reactor temperature and pressure on average char particle size

Press., atm/Temp., ° C	Average Char Particle Diameter*, in.			
	750	800	850	900
69	---	0.0735	0.0628	0.0537
83	---	---	0.0566	0.0501
103	0.0667	---	---	0.0485
205	0.0521	0.0492	0.0529	0.0345

$$\bar{d}_p = \left[ \sum_i \frac{x_i}{d_{p_i}} \right]^{-1}, \text{ Pittsburgh seam hvAb coal, 50 x 100 mesh feed.}$$

The effect of feed rate per unit reactor cross section on the average char particle diameter is shown in Figure 12. As the feed rate is increased for a fixed reactor diameter, the number of particle collisions increase and hence the mean char particle size increases due to agglomeration. At a mass feed rate of 221 lb/hr ft<sup>2</sup>, Pittsburgh seam coal yielded an average char particle diameter of 1.70 mm (0.0669 inches) compared to 0.487 mm (0.0192 inches) for char produced from Illinois #6 hvCb coal under identical reactor conditions. The maximum capacity in the dilute-phase section of the two-stage integrated reactor is limited by the size of the char produced in the dilute phase section that may be fluidized adequately in the second-stage fluid-bed section. Therefore, the dilute-phase reactor capacity will be much higher for Illinois coal than for Pittsburgh coal because of the smaller size char particles produced.

The feed rates per unit area in Figure 12 are probably low because the coal is not completely distributed across the dilute-phase reactor cross section before rapid heat-up and devolatilization, when the coal is susceptible to caking. As mentioned earlier, the coal is fed by a 5/16 inch diameter tube into a 3.26 inch diameter reactor. The particles hit the wall of the reactor about 12 inches down from the end of the feed nozzle. If devolatilization is completed within 6 inches from the end of the nozzle, a feed rate calculated to be 300 lbs/hr ft<sup>2</sup> of reactor cross section actually corresponds to a rate of 1000 lbs/hr ft<sup>2</sup> of cross-sectional area occupied by the particles. Data from a free-fall carbonizer (27), 12 inches in diameter, at the Morgantown Energy Research Center, show that Pittsburgh coal was processed at 1000 lbs/hr ft<sup>2</sup> and yielded char with a mean diameter of about 0.508 mm (0.02 inches). The feed coal was 70 pct through 200 mesh.

The reaction rate constants for the FDP reactor are shown on an Arrhenius plot in Figure 13. The relatively low activation energy of 15.1 kcal/mole of carbon reacted appears to indicate that the reaction may be controlled by mass transfer of hydrogen to the reaction sites and not by the rate of hydrogasification. Feldmann (2) has suggested that in the higher temperature range the rate may be better described as proportional to  $k_g P_{H_2}$ , where  $k_g$  is a mass transfer coefficient for hydrogen through the gas film surrounding the particle. This seems reasonable since a straight line could have just as easily fit the total carbon conversion data in Figures 7 and 8. The activation energy for carbon hydrogasification in an entrained flow reactor was determined by Zahradnik and Glenn (21) to be 15 kcal/mole, in agreement with the value obtained in this work. They suggest that this activation energy represents the difference in activation energy between the hydrogasification and polymerization reactions. An Arrhenius plot of Feldmann's (1) in which he calculates  $k$  by integrating Equation 7 from zero to  $x$  instead of from  $E$  to  $x$ , shows some low temperature FDP data. The activation energy is 29.8 kcal/mole for temperatures below 580° C, and decreases to 6.4 kcal/mole for temperatures above 580° C. The  $k$  values were calculated this way because  $E$  could not be determined from the available data and because  $P_{H_2}$  was approximately constant. This change in activation energy supports Feldmann's suggestion that the reaction is mass transfer controlled. More comments will be made on these results after reviewing some low-temperature "hot-rod" reactor data.

The data presented for the FDP reactor are based mainly on Pittsburgh seam hvAb coal. This coal was studied extensively because of its extreme swelling and agglomerating properties. If the reactor could process badly caking coal than surely it could easily handle mildly caking coals. Illinois #6 hvCb coal is mildly caking and FDP results on this coal are shown in Figure 14. The conversion of Illinois coal has not been studied over a wide range of hydrogen partial pressure as has the Pittsburgh coal, but does appear to be more reactive based on comparison of the two coals in Figure 14 at the same reactor conditions.

"Hot-Rod" Reactors

The results from the "hot-rod" reactor tests of Hiteshue, Friedman, and Madden (7) will be referred to as HR-1 series when coal is used as the starting reactant and HR-1C when char is used. Unpublished data of Feldmann and Williams will be referred to as HR-2 and HR-2C series. The weight loss and carbon conversion data are shown in Figures 15 and 16, respectively, for the HR-2 series experiments. In most of the HR-2 tests the reactor temperature was maintained low enough that Type 2 carbon conversion appeared to occur over a period of about 6 minutes. Once the temperature exceeded about 600° C, Type 3 carbon was rapidly formed. The conversions at which the curves in Figure 15 or 16 appear to level off correspond to the transition points at which the hydrogasification occurs predominately with Type 3 carbon. For the tests at 800° C, the devolatilization and Type 2 carbon conversion both occur in less than a minute. This is more clearly visible when the rate constants are plotted on the same Arrhenius graph with the FDP data in Figure 13. For the data up to 600° C, Equation 4 was integrated starting from zero carbon conversion, and the values of  $k$  and  $\alpha$  were determined from a least-squares fit of the data ( $E$  was found to be very close to zero in the regression analysis for temperatures below 520° C). For the 800° C data, the integration was started from  $E$  with  $\alpha = 1$ , and again  $k$  and  $E$  were determined from a least-squares analysis of the data. The values of these parameters are listed in Table 6. The model was also fit to the total weight loss data in Figure 15. As is obvious in Figure 16, the carbon conversions calculated from the carbon analyses were not consistent at 425° C and 69 atm with either the total conversion data in Figure 15 or data at 35 atm. Therefore, the carbon gasification rate constant at 425° C was calculated by extrapolating the line obtained when  $k$  is plotted versus  $k_T$  (rate constant for total conversion). The  $k$  value at 425° C can also be estimated by assuming the curve must pass through 0.0588 (average of two data points) at 6 minutes. This method gives a  $k$  value of  $0.255 \text{ atm}^{-1} \text{ hr}^{-1}$  compared to  $0.383 \text{ atm}^{-1} \text{ hr}^{-1}$  by extrapolation.

In the Arrhenius plot of Figure 13, the low temperature "hot-rod" reactor data appears to be consistent with the dilute-phase reactor data. Unfortunately, low temperature FDP data is very difficult to obtain in order to verify the low temperature "hot-rod" reactor data because of agglomeration and plugging. The high temperature "hot-rod" reactor data cannot verify the FDP data because the heat-up rate and residence times are such that they operate in different carbon conversion regimes. The key difference between the FDP reactor and the "hot-rod" reactor is the coal heat-up rate. In the FDP reactor this rate is on the order of 1000° C/sec whereas in the "hot-rod" reactor the rate is about 7° C/sec. By achieving reaction temperature quickly enough, the kinetics of Type 2 carbon hydrogasification can be observed.

The carbon conversion data for the HR-1 series experiments are shown in Figure 17. In these tests the devolatilization and Type 2 carbon conversion occurred in less than a minute because of the high temperatures. Therefore the curves for the most part represent Type 3 carbon conversion. Johnson (23) has observed in thermobalance experiments that devolatilization and Type 2 carbon conversion are essentially complete within 2 minutes at temperatures above about 800° C. The heat-up rate in the thermobalance tests was about the same as in the "hot-rod" reactor tests. The HR-1 series data were fit using Equation 4 with  $\alpha = 1$  and integration starting from  $E$ . The kinetic parameters are listed in Table 7. Choosing  $\alpha = 1$  simply means that essentially all the carbon beyond the fraction  $E$  is Type 3. Here  $E$  represents the sum of Types 1 and 2 carbon.

Figure 18 illustrates the effect of the reactor temperature on the amount of carbon that can be hydrogasified as Types 1 and 2. High temperatures and hydrogen

TABLE 6.- Kinetic parameters for HR-2 series data

Temp., ° C	P <sub>H<sub>2</sub></sub> , atm	$\alpha$	E	k atm <sup>-1</sup> hr <sup>-1</sup>	$\alpha_T^{**}$	k <sub>T</sub> <sup>**</sup> atm <sup>-1</sup> hr <sup>-1</sup>
425	69	.071*	0	0.383*	.099	0.510
470	69	.189	0	0.447	.261	0.594
490	69	.199	0	0.625	.278	0.838
520	69	.179	0	1.47	.264	2.07
600	69	.232	0	0.976	.272	1.08
600	69	1.0	.175	0.00751	---	---
800	69	.315	0	1.22	.344	1.66
800	69	1.0	.243	0.0123	---	---

\* Extrapolated using total conversion k<sub>T</sub> values. By another method, the k value is 0.255 atm<sup>-1</sup>hr<sup>-1</sup>.

\*\* Subscript T indicates total conversion parameters (total weight loss).

TABLE 7.- Kinetic parameters for HR-1 series data

Temp., ° C	P <sub>H<sub>2</sub></sub> , atm	$\alpha$	E	k atm <sup>-1</sup> hr <sup>-1</sup>
800	18.0	1.0	.252	0.0282
800	35.0	1.0	.355	0.0154
800	69.0	1.0	.450	0.0169
1200	4.4	1.0	.298	0.363
1200	18.0	1.0	.377	0.137
1200	35.0	1.0	.514	0.350

TABLE 8.- Effect of hydrogen partial pressure on carbon conversion in the hot rod reactor

Test	Temp., ° C	P <sub>H<sub>2</sub></sub> , atm	Carbon Conversion, pct		
			1 min.	2 min.	5-6 min.
HR-1	800	18	---	---	30.7, 25.7
HR-1	800	35	---	---	39.4, 40.4
HR-1	800	69	---	---	52.0, 55.5, 52.6, 54.6
HR-2	500	35	9.10	12.1	---
HR-2	490	69	10.4	14.5	---
HR-2	600	35	17.6	18.4	---
HR-2	600	69	17.5	17.9	---
HR-2	700	35	---	21.0	---
HR-2	800	35	23.7	24.3	31.2
HR-2	800	69	25.6	25.8	33.9

partial pressures result in a large amount of carbon being hydrogasified in the Types 1 and 2 regime. In fact Moseley and Paterson (22) have shown that at a hydrogen partial pressure of 500 atm and 900° C, the carbon is rapidly gasified to completion.

There is a large difference in the level of Types 1 and 2 carbon conversion between the HR-1 data at 800° C and the corresponding HR-2 tests. This discrepancy is shown in Table 8 and is especially noticeable at 800° C and 69 atm. Under these conditions the conversions from the HR-1 tests range from 52 to 54.6 pct at a residence time of 5 minutes whereas the corresponding conversions for the HR-2 tests ranged from 31.2 to 33.9 pct at a residence time of 6 minutes. The lack of response of conversion to changes in hydrogen partial pressure in the HR-2 tests suggests that the reaction rate was strongly mass transfer controlled. This can be verified by comparing the gas velocities in the HR-1 and HR-2 experiments in Table 9. In the HR-1 tests the superficial hydrogen feed gas velocity was 36 cm/sec compared to a velocity of 1 to 2 cm/sec in the HR-2 tests. Apparently the gas velocity was low enough in the HR-2 tests that at the higher temperatures the mass transfer resistance through the particle gas film was significant. In addition, the slower particle heat-up rate may have contributed to the difference in conversions. Anthony (28) has demonstrated, however, that varying the heating rate from 180 to 10,000° C/sec has no effect on the coal conversion. He found smaller particle sizes and more highly dispersed samples to be extremely important because the flux of volatiles emerging from the coal particle may limit the counter diffusion of hydrogen into the particle. This restriction makes it difficult for the hydrogasification reaction to compete with polymerization reactions that produce a relatively inactive char.

In Table 10 the Types 1 and 2 carbon conversion for FDP and "hot-rod" reactor tests are compared. The HR-2 tests were definitely mass transfer controlled whereas it is difficult to conclude this in the FDP tests compared to the HR-1 tests because of the large difference in residence time. In the FDP reactor the residence time was less than 1 second and in the "hot-rod" reactor it was two orders of magnitude greater. Anthony (28) has shown that Types 1 and 2 carbon conversions are complete after about 3 seconds at 69 atm, 900° C, and a heating rate of 750° C/sec. His starting coal particle size was 70 microns compared to about 220 microns in the FDP experiments. Therefore Types 1 and 2 carbon conversion in the FDP tests probably did not reach completion.

Photographs of some of the chars under a scanning electron microscope reveal the porous structure produced in the FDP and "hot-rod" reactors under various conditions. Figure 19 compares chars produced in the FDP reactor at 725° C, 205 atm (top-left), and at 850° C, 69 atm (bottom-left). The char produced at 69 atm appears to be much more porous and less dense than the char made at 205 atm. As discussed previously, this effect shows up as a large difference in bulk density.

Figure 20 compares chars produced in the "hot-rod" reactor at 600° C, 69 atm (bottom) and at 800° C, 69 atm (top) at different residence times. The low temperature char has much larger pores while the high temperature char has a larger number of very small pores. This difference in the pore size is probably related to the higher emission rate of volatile matter from the particles reacted at 800° C. In addition, the superficial hydrogen velocity in the 600° C test was 0.9 cm/sec versus 1.1 cm/sec in the 800° C test. Both these conditions (high volatiles emission, low gas velocity) limit counterdiffusion of hydrogen into the char structure resulting in less competition for the polymerization reaction. Comparison of the FDP and "hot-rod" char samples indicates that the pore structure of the FDP char is more highly developed with pores having thin walls. The samples in Figure 20 were crushed to 100 pct thru 60 mesh so that the gross pore structure is not as clear as possible.

TABLE 9.- Effect of hydrogen velocity on carbon conversion  
in the hot rod reactor at 800° C

<u>Series</u>	<u>Sample</u>	<u>P<sub>H<sub>2</sub></sub>, atm</u>	<u>H<sub>2</sub> velocity cm/sec</u>	<u>Average Carbon Conv., %</u>	<u>Residence Time, min.</u>
HR-1	Pgh. hvAb Coal	35	36.6	39.9	5
HR-2	Pgh. hvAb Coal	35	2.19	31.2	6
HR-1	Pgh. hvAb Coal	69	36.6	53.7	5
HR-2	Pgh. hvAb Coal	69	1.11	33.9	6
HR-1C	Pgh. hvAb Char	69	36.6	31.4	15
HR-2C	Ill. #6 hvCb Char	69	1.11	31.2	15

TABLE 10.- Comparison of types 1 and 2 carbon conversion  
in the FDP and "Hot-Rod" Reactors

<u>Tests</u>	<u>P<sub>H<sub>2</sub></sub>, atm</u>	<u>Carbon Conv., %</u>
FDP*	35.0	27.2
FDP*	69.0	32.2
HR-1**	35.0	33.2, 32.8
HR-1**	69.0	38.5, 40.3
HR-2**	35.0	23.7
HR-2**	69.0	25.6

\*From Figure 8, 850°-900° C.

\*\*800° C.

TABLE 11.- Kinetic parameters for HR-1C series data

<u>Temp., ° C</u>	<u>P<sub>H<sub>2</sub></sub>, atm</u>	<u>α</u>	<u>E</u>	<u>k atm<sup>-1</sup>hr<sup>-1</sup></u>
800	18.0	1.0	.009	.0234
800	35.0	1.0	.027	.0178
800	69.0	1.0	.144	.0110
800	69.0	1.0	.136	.0137*

\*HR-2C data.

Figure 21 shows the char samples from FDP tests at 850° C and 69 atm using a lignite coal feed. The pore structure appears very undeveloped compared to the structure obtained with bituminous coal. Because of the lack of particle swelling with lignite (coal particle also in Figure 21), the penetration of hydrogen into the particle is poorer compared to bituminous coal. Consequently, particle size should have an even stronger influence on the hydrogasification of lignite than with bituminous coals.

The char data in Table 9 are very interesting because the superficial hydrogen velocity had no effect on the carbon conversion. The mass transfer rate into the char particles must be large compared to the char-hydrogen reaction rate. This is not surprising since the reaction rate of Type 3 carbon is very slow, probably much slower than the diffusion rates of hydrogen and gaseous reaction products.

The results of HR-1C series experiments with char produced from Pittsburgh seam hvAb coal are shown in Figure 22. The carbon conversion is of the Type 3 species except for a small amount of rapid initial conversion. The kinetic parameters for these data are listed in Table 11. The results of the HR-2C series experiments are also shown in Table 11 and Figure 22, and agree well with the HR-1C data. The two chars are different in that the HR-2C char was produced from Illinois #6 hvCb coal in the dilute phase reactor at 585° C whereas the HR-1C char was produced from Pittsburgh seam hvAb coal by batch carbonization for 2 hours in helium at 600° C. The HR-2C char contained about 26 pct volatile matter compared to the original 36.5 pct volatile matter in the starting coal. Despite these differences, except for the nearly equal devolatilization temperatures, the reactivities of the two chars are essentially the same. A significant difference in the devolatilization temperatures could have resulted in the chars having differing reactivities (23, 29).

The Arrhenius graph in Figure 13 summarizes the results for all the coals and chars tested and includes some of Johnson's data (23) which was adjusted to calculate k values according to Equation 4. Assuming that it is valid to represent the low temperature "hot-rod" reactor data by the same Arrhenius line as the FDP data, the activation energy for hydrogasification of Type 2 carbon is 15.1 kcal/mole of carbon gasified. The hydrogasification rate of Type 3 carbon is about three orders of magnitude lower than the rate of hydrogasification of Type 2 carbon. The activation energy for the HR-1, HR-1C, and HR-2C data is 24.7 kcal/mole of carbon gasified (Type 3 carbon) compared to a value of 47.1 kcal/mole obtained by Johnson (23) using a thermo-balance. At 600° and 800° C, the HR-2 data was complicated by the transition to Type 3 carbon conversion and a significant amount of mass transfer resistance. At these higher temperatures the apparent activation energy falls off considerably as shown in Figure 13.

#### Two-Stage Integrated Reactor

The results of the two-stage tests where the first-stage was a FDP reactor and the second-stage either a moving-bed or fluid-bed reactor have been presented elsewhere (18). The kinetic results are summarized in Tables 12, 13, and 14 and are also plotted in Figure 13. Because heat transfer limitations within the char particles caused the true particle temperature to be higher than the measured temperature, the activation energy of the moving bed data is low, and the rate constant values are relatively high at the lower reactor temperatures.

#### Correlation of Char Yield and Coal H, N, S, and O Conversion Data

In order to predict the conversion of other constituents in the coal during hydrogasification besides carbon conversion, results from ninety-five experiments

TABLE 12.- Kinetic results from two-stage integrated reactor  
experiments (18) at 69 atm

<u>Run</u>	<u>Total C</u> <u>Conv., X</u>	<u>Moving</u> <u>Bed C</u> <u>Conv., Z*</u>	<u>Fluid</u> <u>Bed C</u> <u>Conv., Z*</u>	<u>Bed</u> <u>Temp., °K</u>	<u>k</u> <u>atm<sup>-1</sup>hr<sup>-1</sup></u>
2	0.552	---	0.378	1158	0.0145
3	0.536	---	0.356	1158	0.0284
5	0.558	---	0.345	1158	0.0316
11	0.608	---	0.419	1073	0.0450
12	0.551	---	0.335	1118	0.0202
13	0.556	---	0.383	1113	0.0218
14	0.537	---	0.357	1183	0.0139
33	0.620	0.457	---	1178	0.0573
37	0.392	0.131	---	1173	0.0360
38	0.485	0.264	---	1148	0.0396
39	0.417	0.167	---	918	0.0449
43b	0.430	0.186	---	1038	0.0395
44b	0.391	0.130	---	923	0.0260
45b	0.406	0.151	---	933	0.0307
46a	0.399	0.151	---	957	0.0305
48	0.511	0.301	---	1073	0.0299
49	0.536	0.337	---	988	0.0358

TABLE 13.- Hydrogasification of Illinois #6 hvCb coal in a two-stage reactor at 1000 psig - run conditions

Test	46		48		49	
Reactor Zone	FDP*	MB*	FDP	MB	FDP	MB
Temp., ° C	850	684	850	800	850	715
Coal or Char Rate, lb(dry)/hr	10.51	6.68	10.26	5.08	10.32	5.01
Bed Height, in.	---	0	---	36	---	36
Residence Time, min.	---	0	---	10.4	---	10.4
Feed Gas, SCFH	164.4	141.4	181.7	152.0	166.2	150.7
Vol. Pct. H <sub>2</sub>	56.2	99.4	52.0	99.0	50.9	98.6
CH <sub>4</sub>	37.2	---	42.1	---	42.8	---
N <sub>2</sub>	1.05	0.50	1.10	1.00	1.50	1.30
He	5.45	---	4.70	---	4.70	---
Product Gas, SCFH**	168.6	141.4	179.0	124.6	169.8	130.3
Vol. Pct. H <sub>2</sub>	34.8	99.4	32.4	54.2	30.1	58.0
CH <sub>4</sub>	55.1	---	57.2	43.5	58.0	39.0
Run Time, min.	187		193		187	

\* FDP: free-fall dilute phase reactor (3 foot heated length); MB: moving-bed reactor.

\*\*For runs 48 and 49, the individual product gas flowrates and the composition of the MB product gas prior to mixing were estimated using the helium tracer data.

TABLE 14.- Hydrogasification of Illinois #6 hvCb coal in a two-stage reactor at 1000 psig - results

Test HY	46	48	49
Conversion, wt. pct.			
MAF Coal	43.1	60.2	60.4
C	33.0	50.7	53.6
H	75.4	96.4	93.4
S	66.7	74.8	76.3
N	59.4	89.7	86.4
O	91.0	99.6	90.0
Gas Yields, SCF/lb dry coal			
CH <sub>4</sub>	3.01	7.80	7.58
C <sub>2</sub> H <sub>6</sub>	0.11	0.17	0.13
CO	0.43	0.69	0.80
CO <sub>2</sub>	0.10	0.09	0.11
H <sub>2</sub>	-3.21	-11.63	-10.31
H <sub>2</sub> S*	0.04	0.03	0.07
Oil Yield, lb/lb dry coal	0.048	0.041	0.026
Carbon to Gas and Oils, wt. pct.	24.3	47.7	44.2
Mean Char Particle Diameter, mm	0.433	---	0.397

\* About 50% of the converted sulfur appears in the gas product after water scrubbing.

in the FDP reactor and FDP-Fluid Bed integrated reactors were correlated with carbon conversion to yield Figures 23-26. The correlations in Figures 23-25 show that char yield and removal of coal hydrogen and nitrogen can be accurately calculated from carbon conversion, independent of reactor conditions and possibly geometry. For carbon conversions above 20 pct (essentially devolatilization) the oxygen removal usually exceeds 90 pct and can be considered to be complete. The data for sulfur removal are very scattered, possibly because of the error in determining changes in small amounts of sulfur in the coal and char samples. In addition, the hydrogen sulfide that is formed may be in equilibrium with sulfur in the char such that a simple correlation with carbon conversion is not possible.

In Figure 27, the char yields have been recomputed in terms of MAF conversion so that the relationship between carbon conversion and MAF conversion can be shown. A curve is drawn through the data such that it bows away from the unit slope line and passes through (0,0) and (100,100). The data in Figures 23-25 only covered the carbon conversion range 22-55 pct so that for simplicity a straight line was used to fit the data. As the range is widened, however, it becomes obvious that a curve gives a better correlation of the data.

The carbon conversion range covered by the HR-1 and HR-2 series experiments is complete, ranging from 0 to 95 pct. In Figure 28, the MAF conversion is plotted versus carbon conversion and essentially the same curve as used in Figure 27 fits these results. Based on these curves it appears that the correlations of coal constituent conversions with carbon conversion are not only independent of reactor conditions, but also reactor geometry. Figure 29 shows a similar MAF-carbon conversion plot for the HR-1C and HR-2C series char tests. The carbon conversion in Figure 29 does not include the carbon that was lost during devolatilization of the coal to prepare the char.

The conversion of coal H, N, and S in the HR-1 and HR-2 series experiments are shown in Figures 30-32. In Figures 30 and 31, the straight line fits of the H and N data determined previously are shown to be inadequate over a very wide range of carbon conversion. These sets of data are both fit best with curves that are concave downward, similar to the MAF curves. Despite the scatter in the data, the correlation with carbon conversion still appears to be valid. Unlike in the FDP and Two-Stage reactor experiments, ultimate analyses were not run on the coal feed for each test, but only on the entire batch of coal. Consequently, some segregation in the feeds could have occurred causing scatter in the calculation of the H, N, and sulfur conversions. These constituents are present in relatively small amounts and thus their calculated conversions are very sensitive to fluctuations in the feed composition. The sulfur data in Figure 32 shows a more definite trend with carbon conversion than was evident in Figure 26 and shows the latter correlation to be conservative. Work is planned to extend the linear correlations in Figures 23-26 to a regression curve that will fit all of the data, i.e., FDP, HR-1, HR-2, and the Two-Stage reactors. These relationships are very valuable in scale-up design calculations because the displacement of the volatile elements in the coal and the char yield can be accurately predicted for the plant flowsheet.

## NOMENCLATURE

- $\alpha$  fraction of the carbon that is available for reaction in the regime being considered.
- $\alpha_T$  fractional weight loss that can be achieved in the reaction regime being considered.
- $\beta$  same as  $\alpha$  except the Type 1 carbon is excluded.
- $\lambda$  stoichiometric coefficient for the char-hydrogen reaction.
- $\mu_g$  gas viscosity, lb/ft hr.
- $\rho_b$  char bulk density, lb/ft<sup>3</sup>.
- $\rho_g$  gas density, lb/ft<sup>3</sup>.
- $\rho_s$  char particle density, lb/ft<sup>3</sup>.
- $\bar{d}_p$  mean char particle diameter, in.
- $E$  fraction of carbon instantaneously devolatilized.
- $g$  gravitational acceleration, ft/sec<sup>2</sup>.
- $k$  char-hydrogen reaction rate constant, atm<sup>-1</sup> hr<sup>-1</sup>.
- $k_T$  weight loss reaction rate constant, atm<sup>-1</sup> hr<sup>-1</sup>.
- $L$  reactor length, ft.
- $P_{H_2}$  partial pressure of hydrogen, atm.
- $Re_p$  char particle Reynolds number.
- $t$  time, sec.
- $U_T$  free-fall velocity of char particles, fps.
- $U_{TS}$  single char particle terminal velocity, fps.
- $W$  coal mass feed rate, lb/hr ft<sup>2</sup>.
- $x$  fractional carbon conversion based on total coal carbon.
- $z$  fractional carbon conversion based on starting char carbon.

References

1. Feldmann, H. F., C. Y. Wen, W. H. Simons, and P. M. Yavorsky. Supplemental Pipeline Gas From Coal by the HYDRANE Process. Presented at the 71st National AIChE Meeting, Dallas, Texas, Feb. 20-23, 1972.
2. Feldmann, H. F. and P. M. Yavorsky. The HYDRANE Process. Presented at the 5th AGA/OCR Synthetic Pipeline Gas Symposium, Chicago, Illinois, Oct. 29-31, 1973.
3. Wen, C. Y., C. T. Li, S. H. Tscheng, and W. S. O'Brien. Comparison of Alternate Coal Gasification Processes for Pipeline Gas Production. Presented at the 65th Annual AIChE Meeting, New York, New York, Nov. 26-30, 1972.
4. Wen, C. Y., coworkers. Optimization of Coal Gasification Processes, Research and Development Rept. No. 66, Interim Rept. Nos. 1 and 2, O.C.R., U.S. Dept. of the Interior, Wash., D. C.
5. Feldmann, H. F., W. H. Simons, J. A. Mima, and R. W. Hiteshue. Reaction Model for Bituminous Coal Hydrogasification in a Dilute Phase. Preprints of Fuel Division, ACS, v. 14, No. 4, Part II, Sept. 1970, pp. 1-13.
6. Feldmann, H. F., J. A. Mima, and P. M. Yavorsky. Pressurized Hydrogasification of Raw Coal in a Dilute-Phase Reactor. Fuel Gasification, Advances in Chem. Series 131, ACS, Washington, D. C., 1974, pp. 108-125.
7. Hiteshue, R. W., S. Friedman, and R. Madden. Hydrogasification of High-Volatile A Bituminous Coal. U.S. Bureau of Mines Report of Investigation 6376, 1964.
8. Hiteshue, R. W., R. B. Anderson, and M. D. Schlesinger. Hydrogenating Coal at 800° C. Ind. & Eng. Chem., 49 (Dec., 1957), pp. 2008-10.
9. Hiteshue, R. W., P. S. Lewis, and S. Friedman. Gaseous Hydrocarbons from Coal. Paper presented at the A.G.A. Operating Section Conference, 1960 (CEP-60-9).
10. Hiteshue, R. W., S. Friedman, and R. Madden. Hydrogenation of Coal to Gaseous Hydrocarbons. U.S. Bureau of Mines Report of Investigation 6027, 1962.
11. Friedman, S., R. W. Hiteshue, and M. D. Schlesinger. Hydrogenation of New Mexico Coal at Short Residence Time and High Temperature. U.S. Bureau of Mines Report of Investigation 6470, 1964.
12. Hiteshue, R. W., R. B. Anderson, and S. Friedman. Gaseous Hydrocarbons by Hydrogenation of Coals and Chars. Ind. & Eng. Chem., 52 (July, 1960), pp. 577-9.
13. Hiteshue, R. W., S. Friedman, and R. Madden. Hydrogasification of Bituminous Coals, Anthracite, and Char. U.S. Bureau of Mines Report of Investigation 6125, 1962.
14. Kawa, W., R. W. Hiteshue, W. A. Budd, S. Friedman, and R. B. Anderson. Agglomeration Studies in the Low-Pressure Hydrogenation of Coal in a Fluidized Bed. U.S. Bureau of Mines Bulletin 579, 1959.
15. Lewis, P. S. and R. W. Hiteshue. Hydrogenating Coal in the Entrained State. Ind. & Eng. Chem., 52 (Nov., 1960), pp. 919-20.
16. Lewis, P. S., S. Friedman, R. W. Hiteshue. High Btu Gas by the Direct Conversion of Coal. Fuel Gasification Advances in Chem. Series 69, ACS, Washington, D. C., 1967, pp. 50-63.

17. Hiteshue, R. W. The Hydrogasification of Raw Coal. Paper presented at the Amer. Gas Assoc. Symposium on Synthetic Pipeline Gas, Pittsburgh, Pa., Nov. 15, 1966.
18. Wen, C. Y., S. Mori, J. A. Gray, and P. M. Yavorsky. Application of the Bubble-Assemblage Model to the HYDRANE Process Fluid-Bed Hydrogasifier. Paper presented at the 67th Annual AIChE Meeting, Wash., D. C., Dec. 1-5, 1974.
19. Feldmann, H. F., W. H. Simons, C. Y. Wen, and P. M. Yavorsky. Simulation of a Reactor System for the Conversion of Coal to Methane by the HYDRANE Process. Paper presented at the 4th International Congress of Chem. Eng., Marianske Lazne, Czechoslovakia, Sept. 11-15, 1972.
20. Given, P. H. The Distribution of Hydrogen in Coals and Its Relation to Coal Structure. *Fuel*, 39 (1960), pp. 147-153.
21. Zahradnik, R. L. and R. A. Glenn. The Direct Methanation of Coal. *Fuel* 50, No. 1, (1971), pp. 77-90.
22. Moseley, F. and D. Paterson. The Rapid High-Temperature Hydrogenation of Coal-Chars Part 2: Hydrogen Pressures up to 1,000 Atmospheres. *J. Inst. of Fuel*, 38 (Sept., 1965), pp. 378-391.
23. Johnson, J. L. Kinetics of Bituminous Coal Char Gasification with Gases Containing Steam and Hydrogen. *Fuel Gasification, Advances in Chem. Series 131*, ACS, Wash., D. C., 1974, pp. 145-178.
24. Kunii, D. and O. Levenspiel. *Fluidization Engineering*. John Wiley & Sons, Inc., New York, 1969, p. 76.
25. Wen, C. Y. and J. Huebler. Kinetic Study of Coal Char Hydrogasification, Rapid Initial Reaction. *Ind. & Eng. Chem. Design & Develop.*, 4 (April, 1965), pp. 142-147.
26. Feldmann, H. F., K. D. Kiang, and P. M. Yavorsky. Fluidization Properties of Coal Char. *Preprints of Fuel Division, ACS*, v. 15, No. 3, Sept. 1971, pp. 62-76.
27. Quarterly Technical Progress Report, Morgantown Energy Research Center, Morgantown, West Virginia, September-December, 1969, p. 2.
28. Anthony, D. B. Rapid Devolatilization and Hydrogasification of Pulverized Coal. Sc.D. Thesis, Dept. of Chem. Eng., M.I.T., Cambridge, Mass., Jan., 1974.
29. Blackwood, J. D., B. D. Cullis, and D. J. McCarthy. Reactivity in the System Carbon-Hydrogen-Methane. *Aust. J. Chem.* 20 (1967), pp. 1561-70.

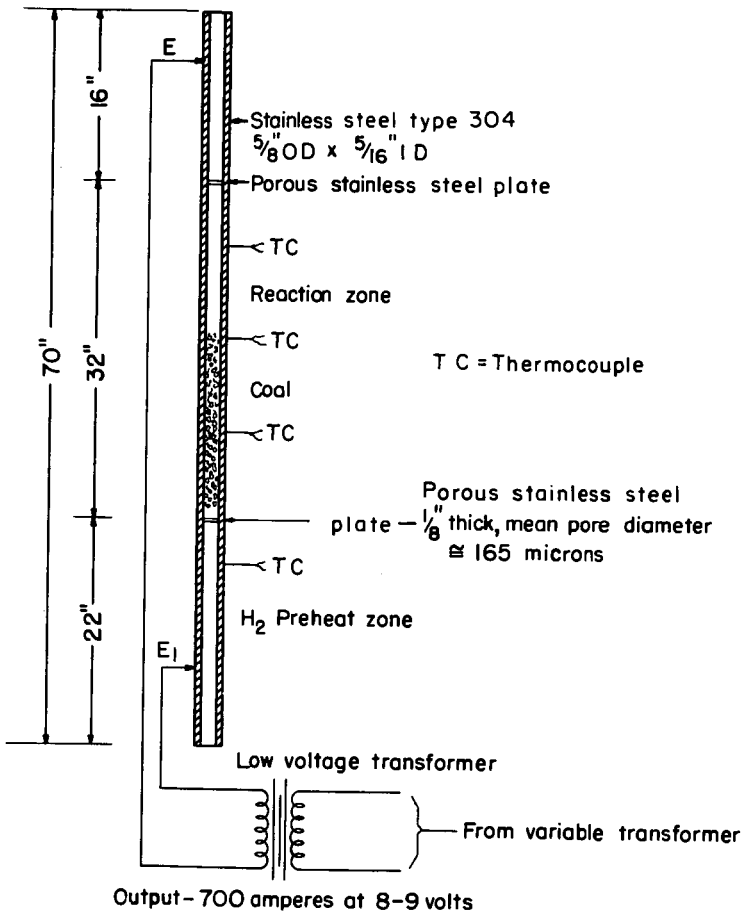
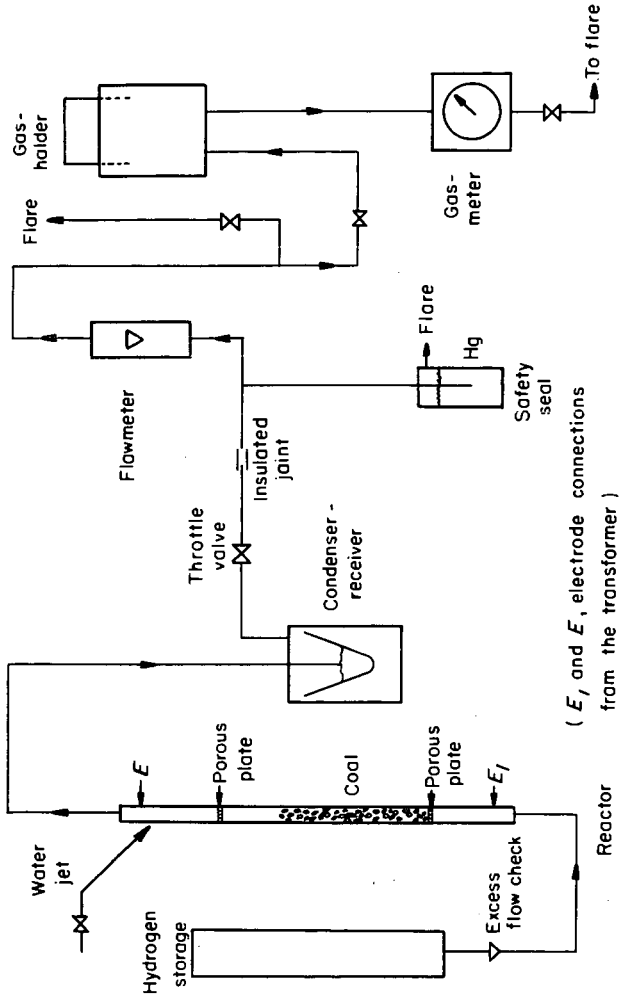


Figure 1 - "Hot-rod" reactor.

L-4753  
 12-12-56



(  $E_1$  and  $E_2$  electrode connections from the transformer )

Figure 2 - Flow sheet of "hot rod" apparatus .

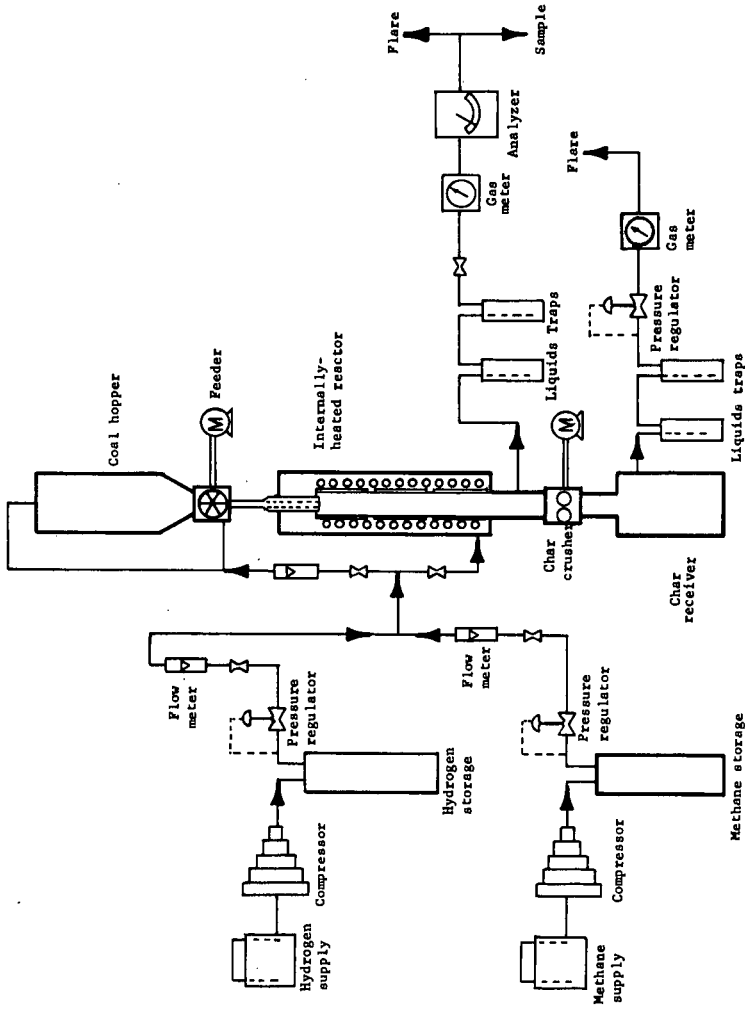


FIGURE 3.- Simplified Flowsheet: Hydrogasification of Coal in Dilute Phase. L-12449

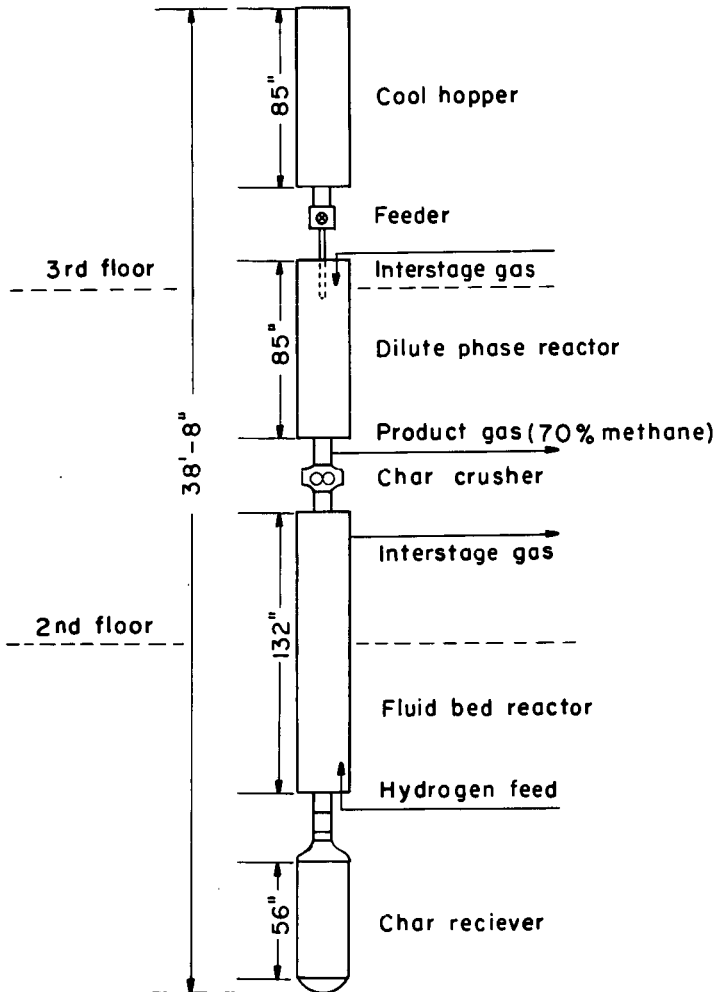


Figure 4 - Integrated hydrogasification unit.

L- 12914

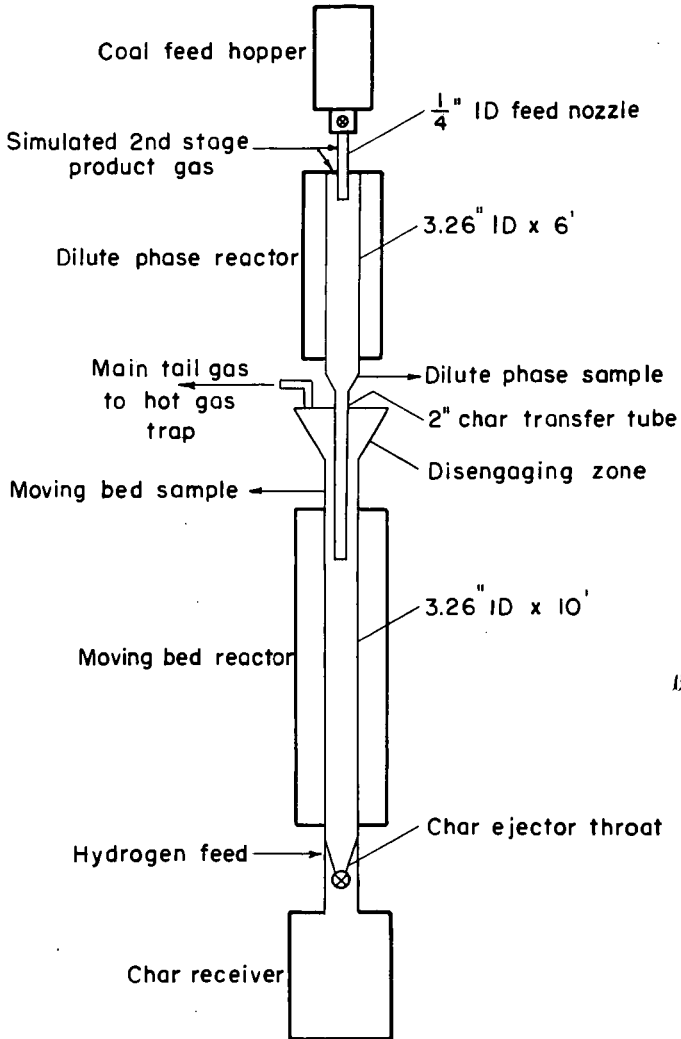


Figure 5 — Integrated two-stage hydrogasifier

L-13753

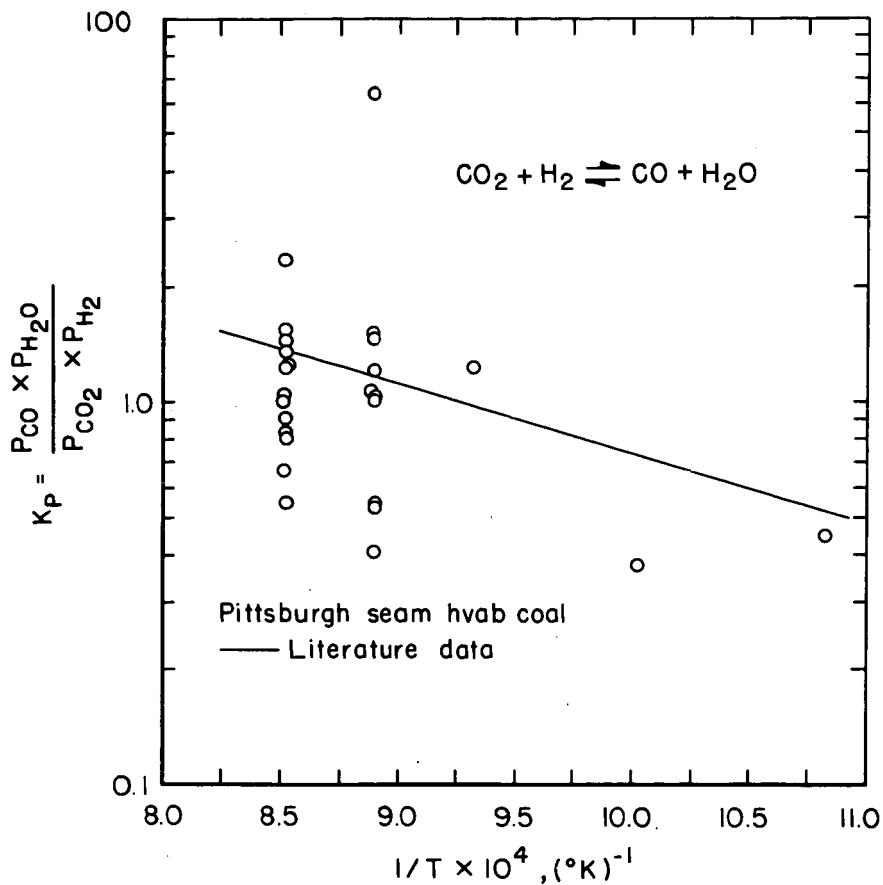


Figure 6- Water-gas shift equilibrium of carbon oxides in the FDP reactor.

5-23-75

L-14298

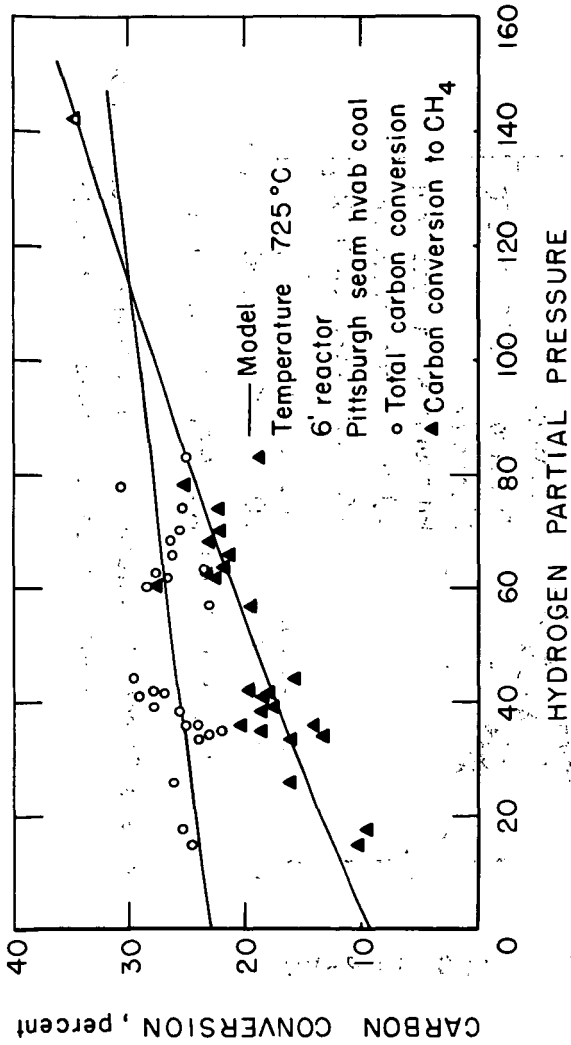


Figure 7 - Effect of hydrogen partial pressure on total carbon conversion and carbon conversion to methane.

5-15-75 L-14296

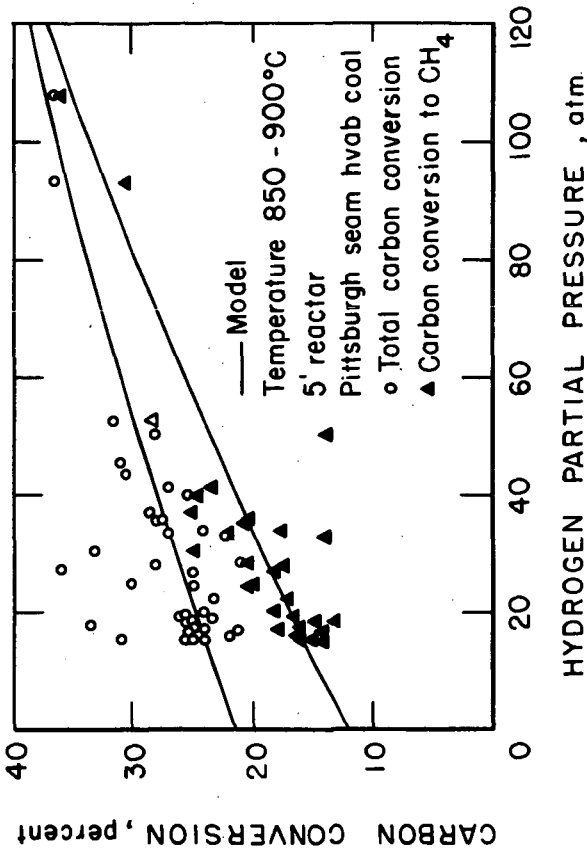


Figure 8-Effect of hydrogen partial pressure on total carbon conversion and carbon conversion to methane.

5-16-75

L-14295

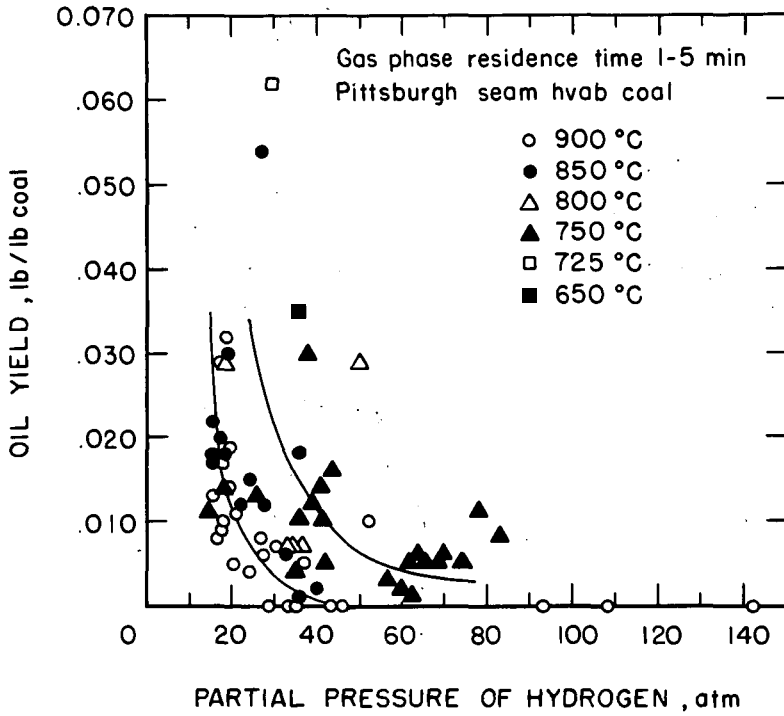


Figure 9 - Effect of hydrogen partial pressure on oil yield.

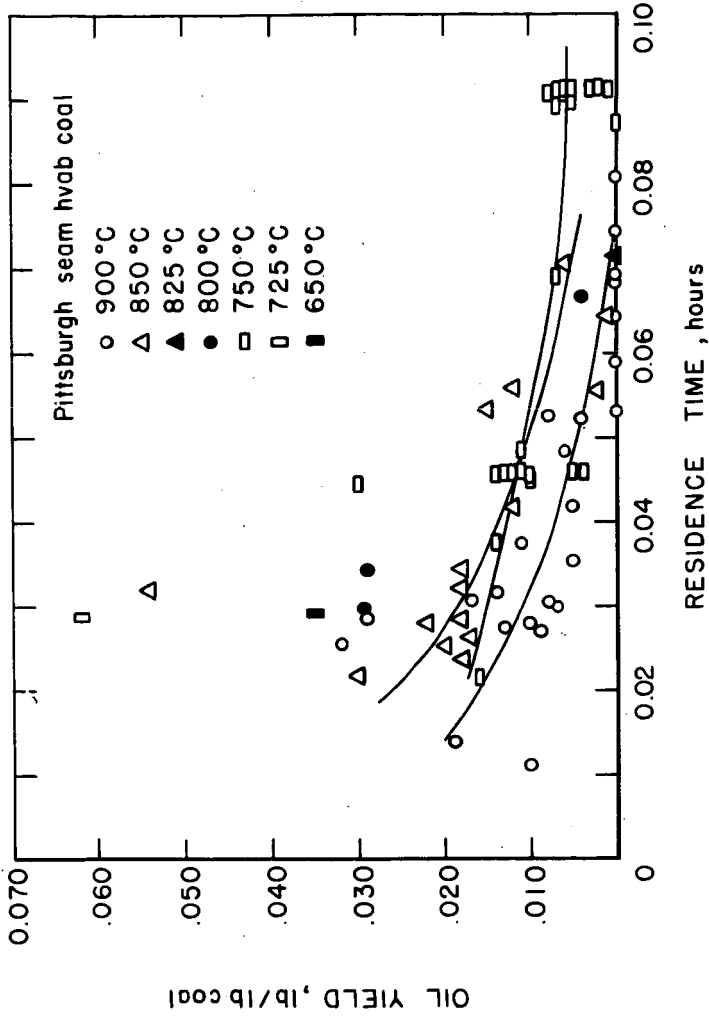


Figure 10-Effect of gas phase residence time on oil yield.

5-21-75

L-14297

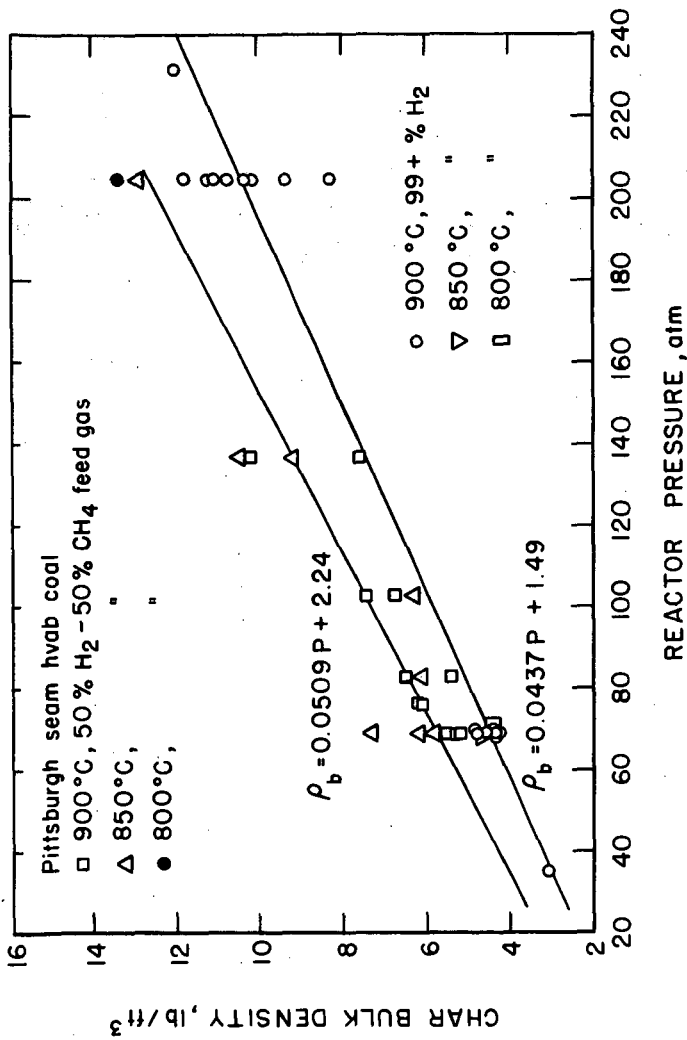


Figure 11 - Effect of total reactor pressure on char bulk density.



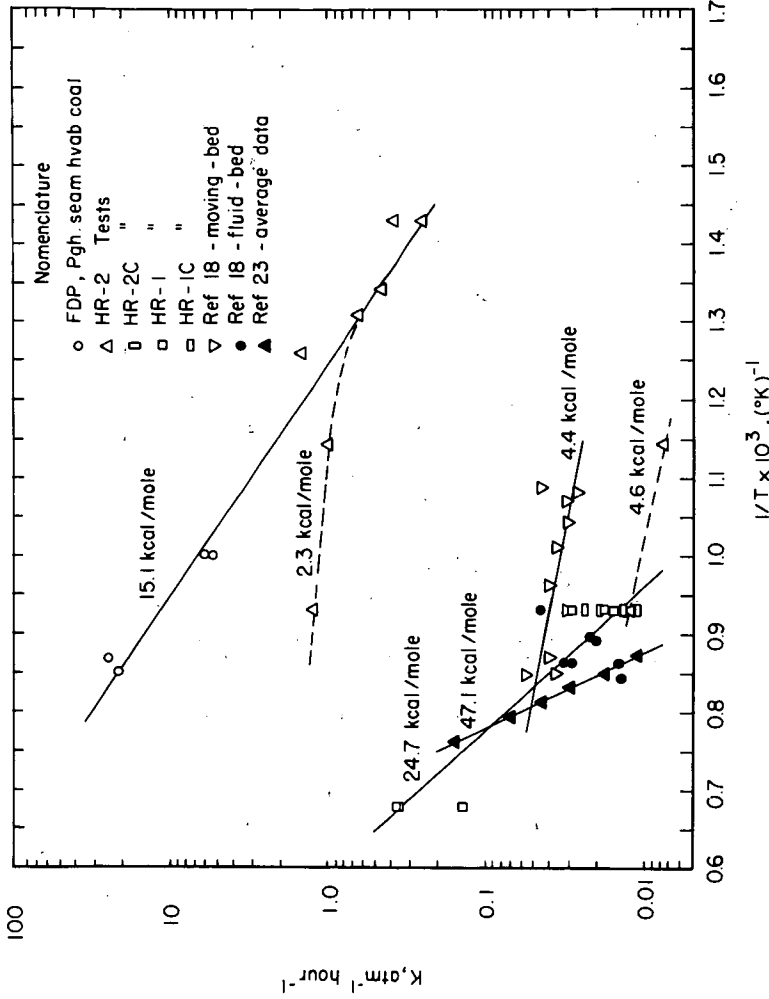


Figure 13 - Temperature dependence of the hydrogasification reactor rate constants for coal and char.

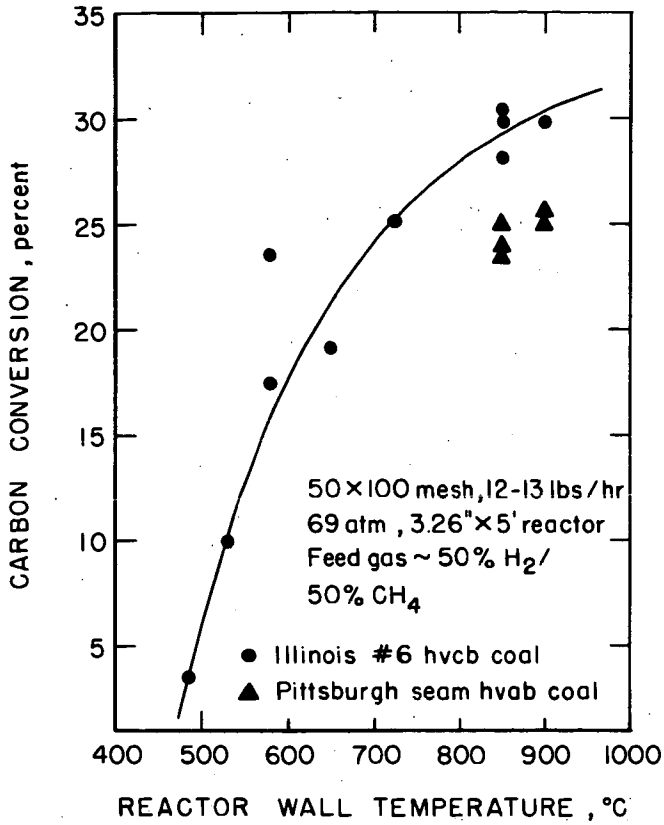


Figure 14 - Carbon conversion in the FDP reactor for Illinois #6 hvcb coal.

5-16-75

L-14292

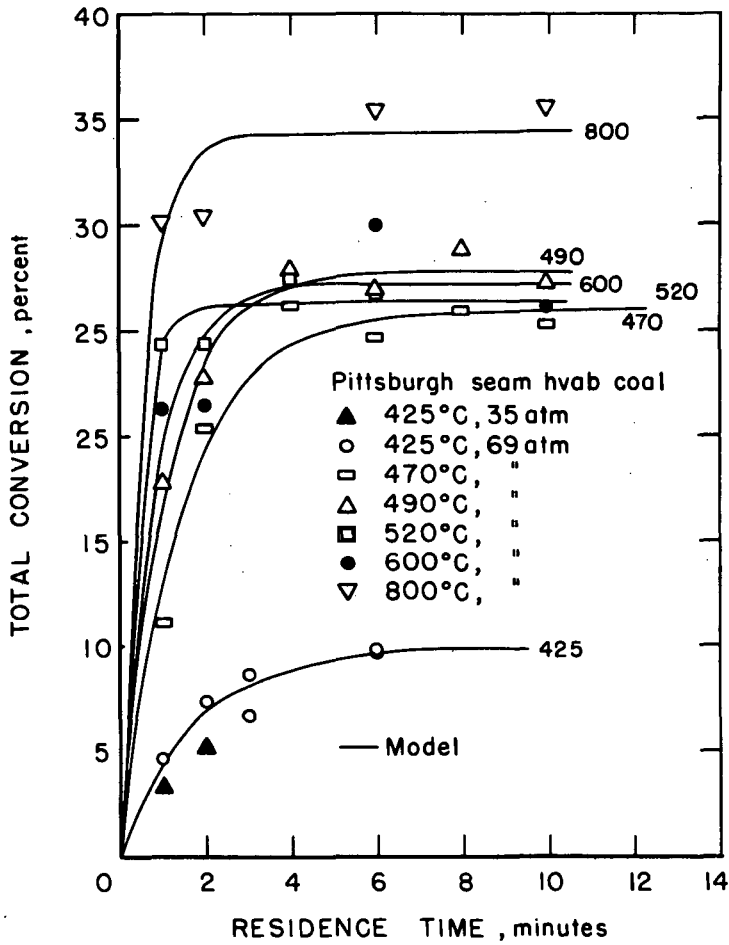


Figure 15 - Effect of temperature and time on total conversion in "hot rod" reactor, HR-2 tests.

5-22-75 L-14300

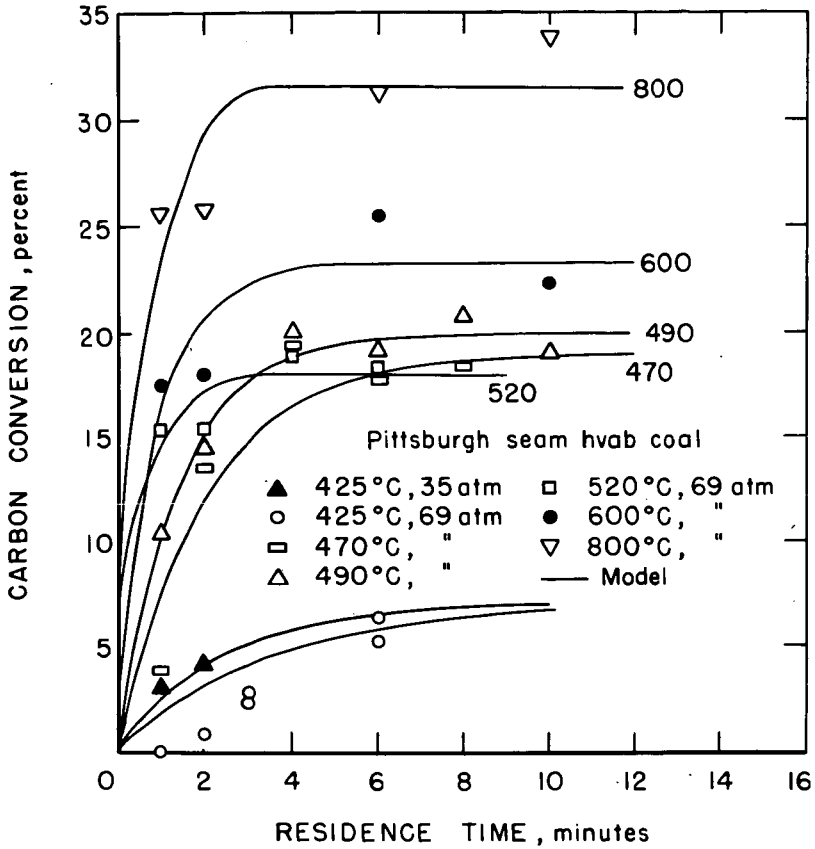


Figure 16- Effect of temperature and time on carbon conversion in "hot rod" reactor, HR-2 tests.

5-27-75 L-14301

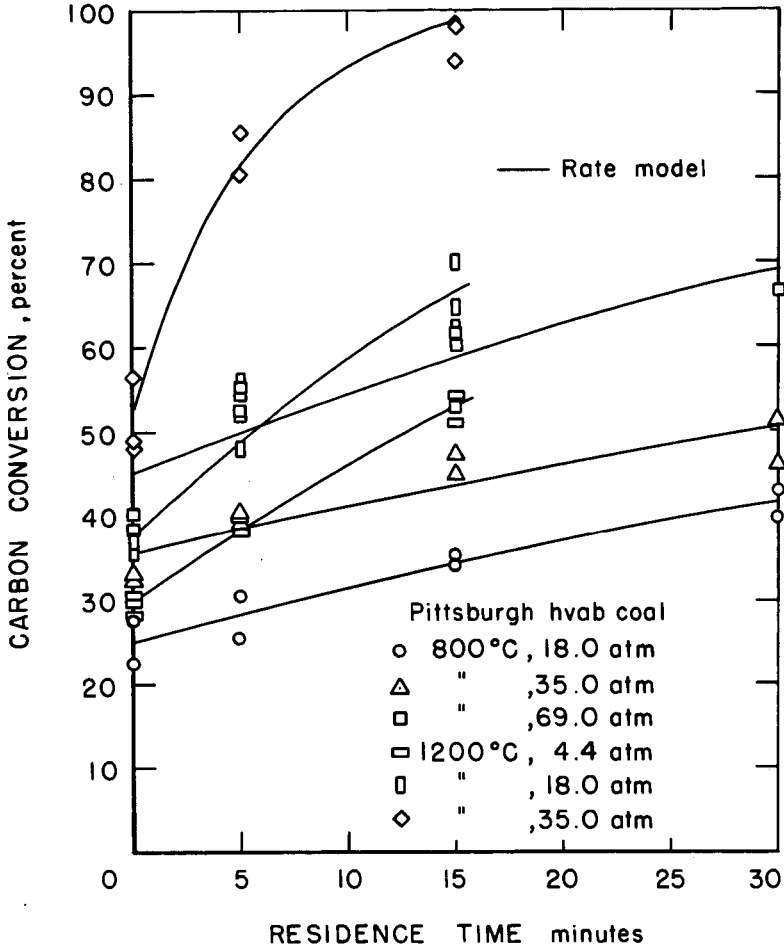


Figure 17- Carbon conversion data for the HR-1 series experiment .

5-21-75 L-14299

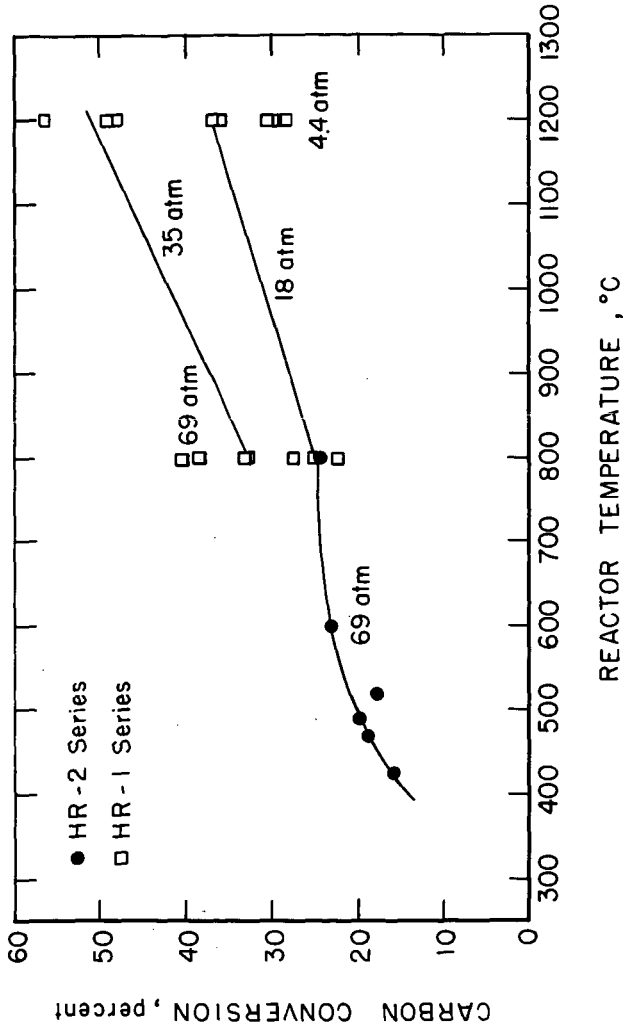


Figure 18-Effect of reactor temperature on types 1 & 2 carbon conversion.

5-15-75 L-14289

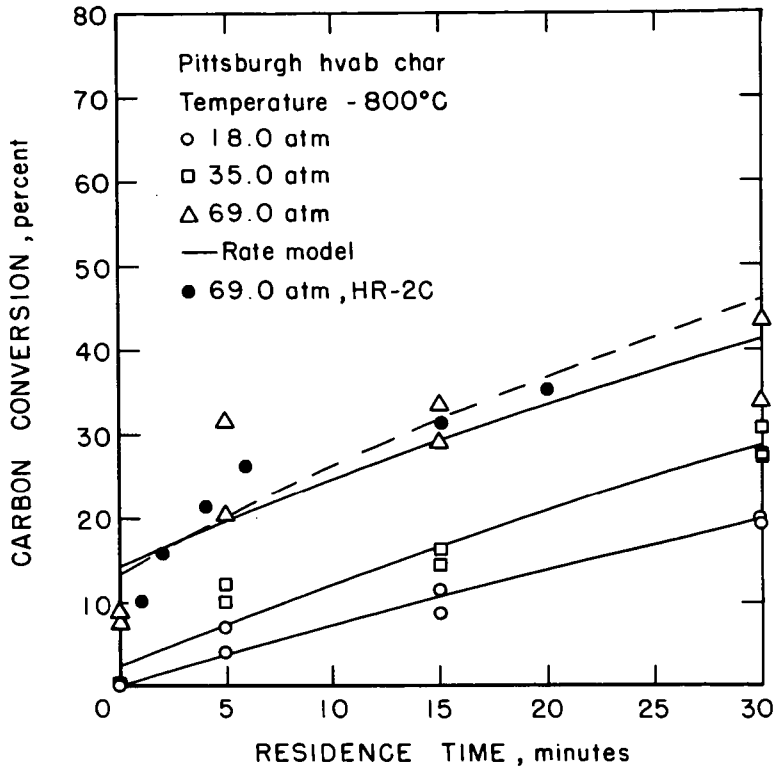


Figure 22- Carbon conversion data for the HR-1C series experiments.

5-15-75

L-14290

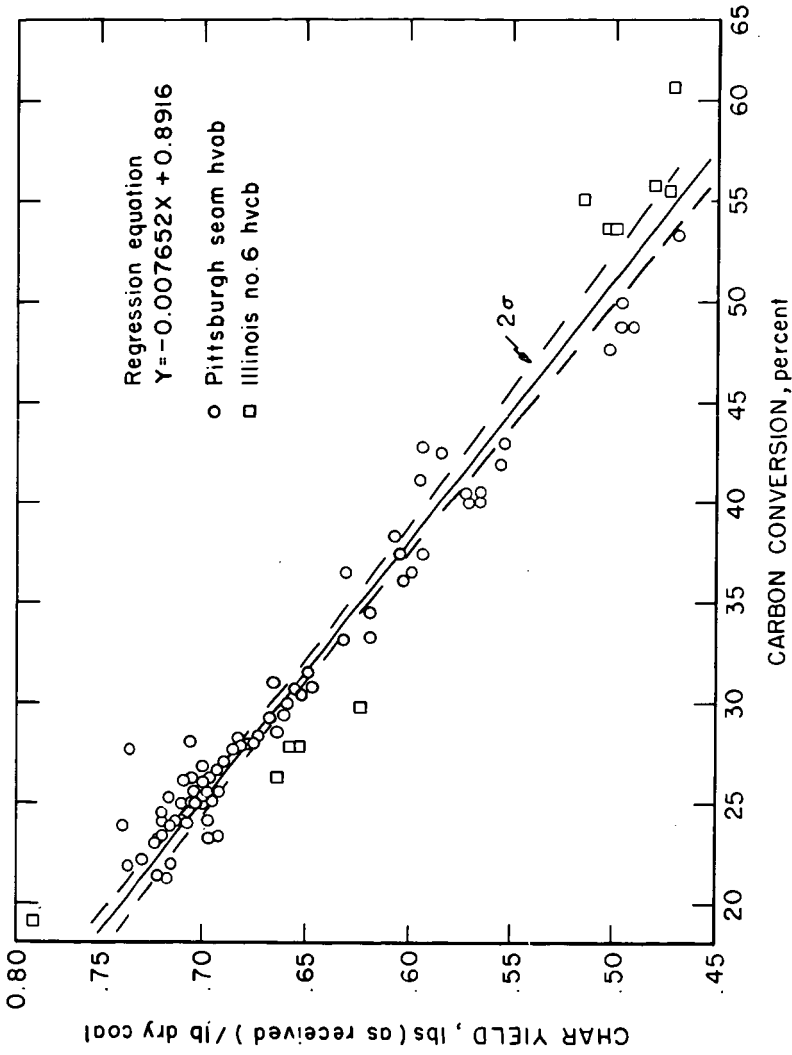


FIGURE 23 - Char yield as a function of carbon conversion during hydrogasification.

L-13708

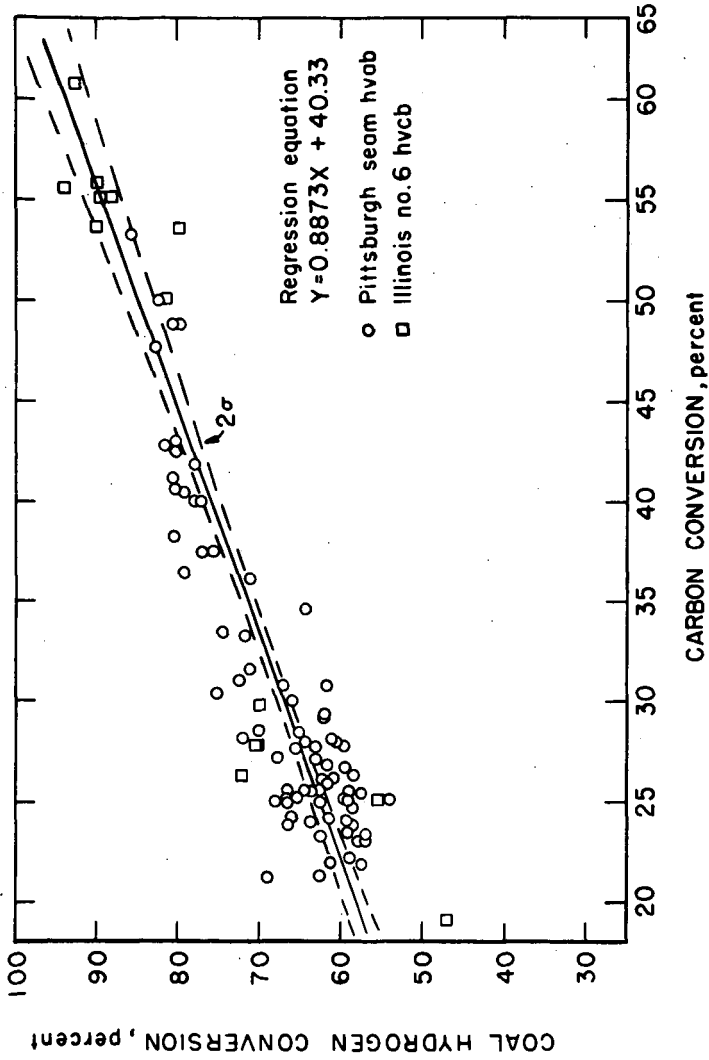


FIGURE 24 - Coal hydrogen conversion as a function of carbon conversion during hydrogosisification.

L-13709

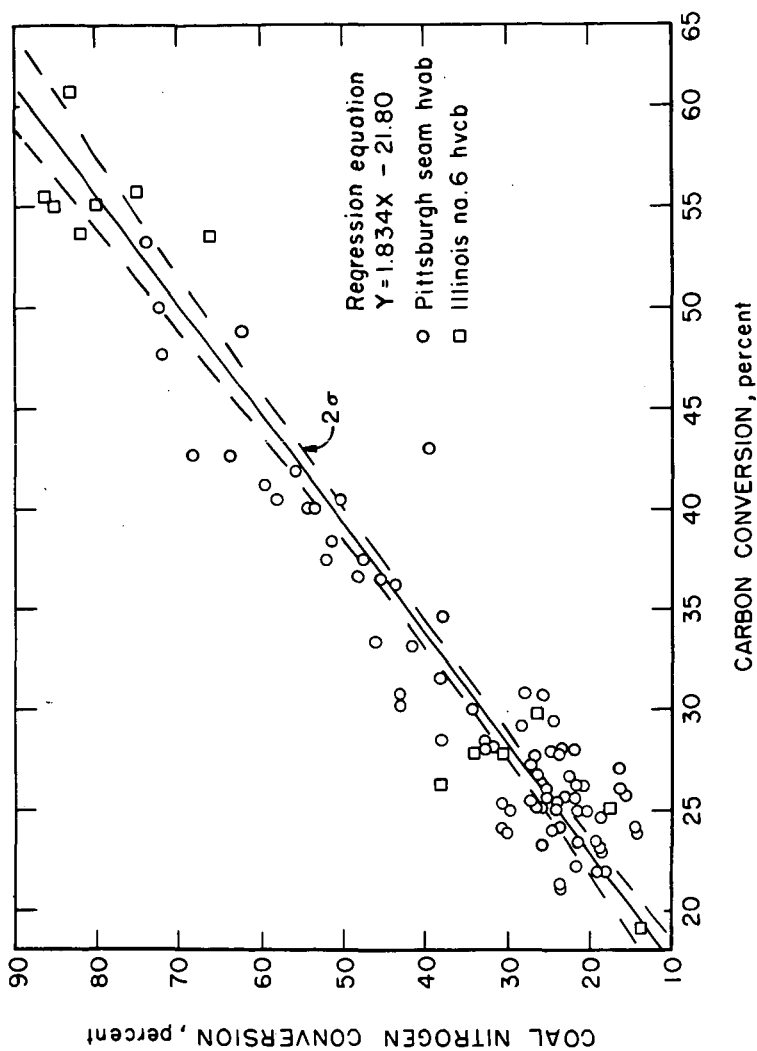


FIGURE 25-Cool nitrogen conversion as a function of carbon conversion during hydrogasification.

L-13712

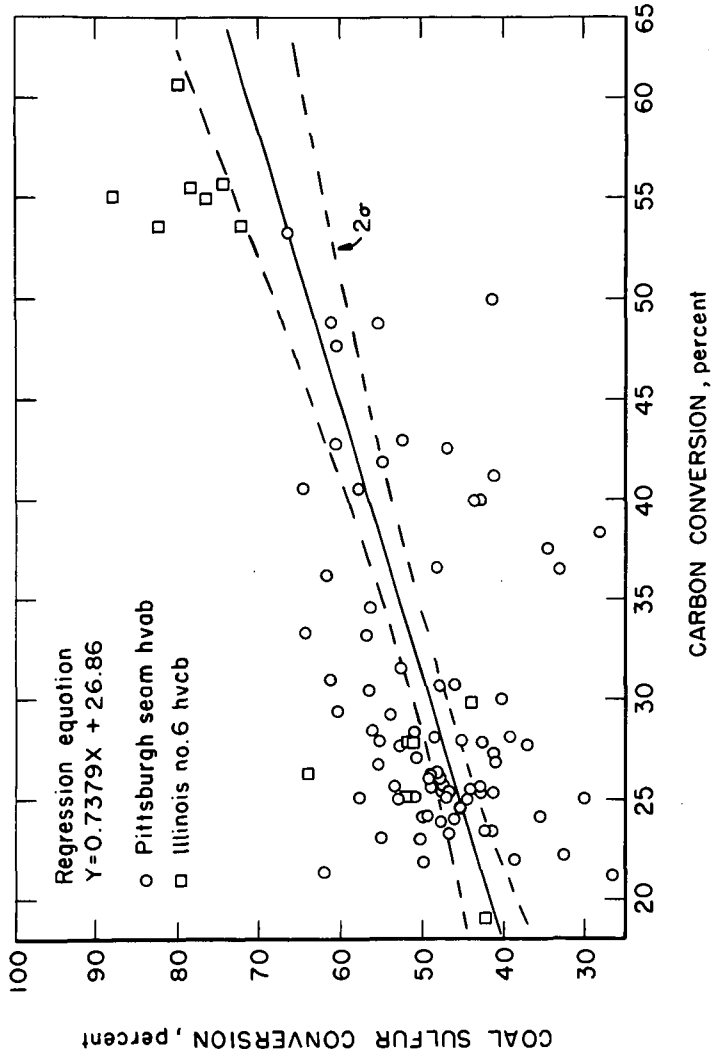


FIGURE 26-Sulfur conversion as a function of carbon conversion during hydrogossification.

L-13710

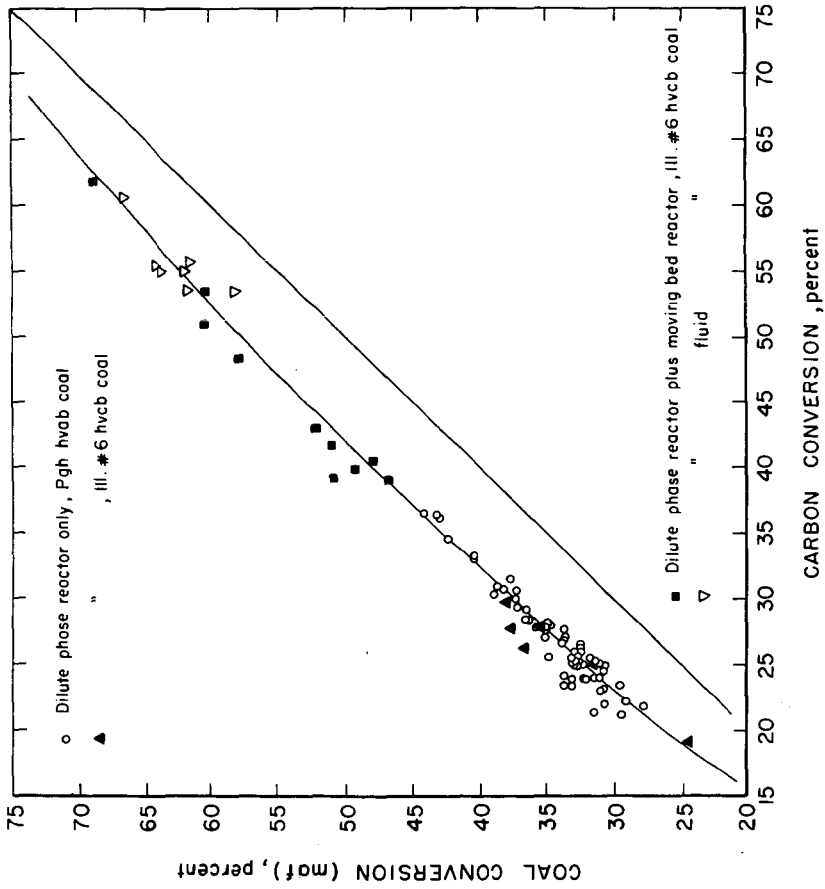


Figure 27-Coal conversion (maf) as a function of carbon conversion during hydrogasification.

5-23-75 L-14305

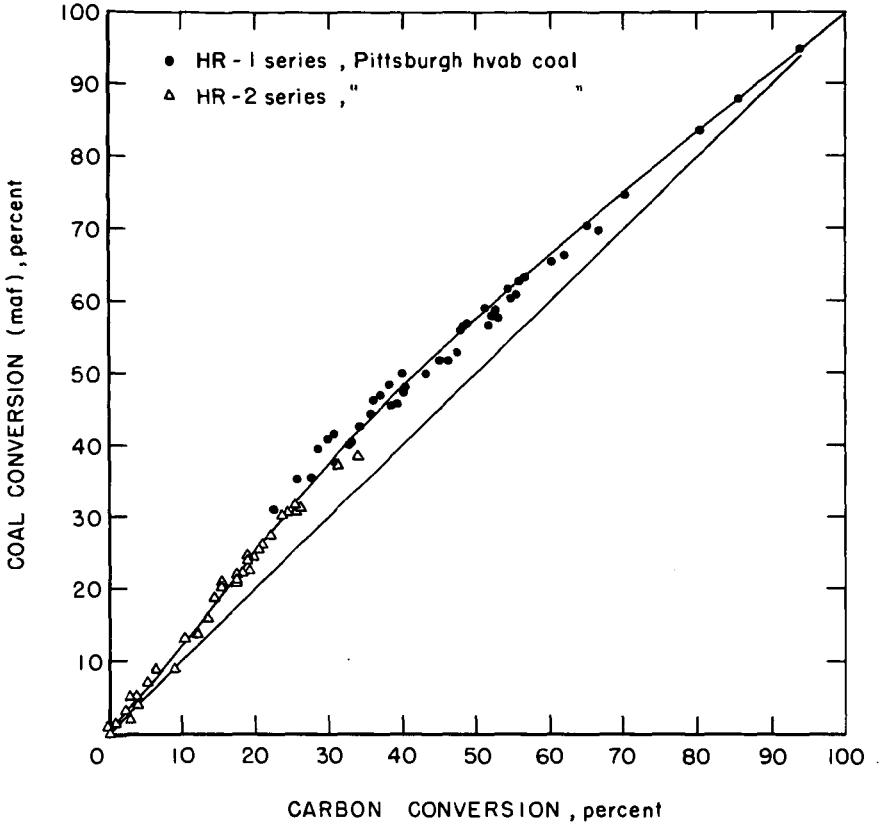


Figure 28 - Coal conversion (maf) as a function of carbon conversion during hydrogasification.

5-16-75

L-14306

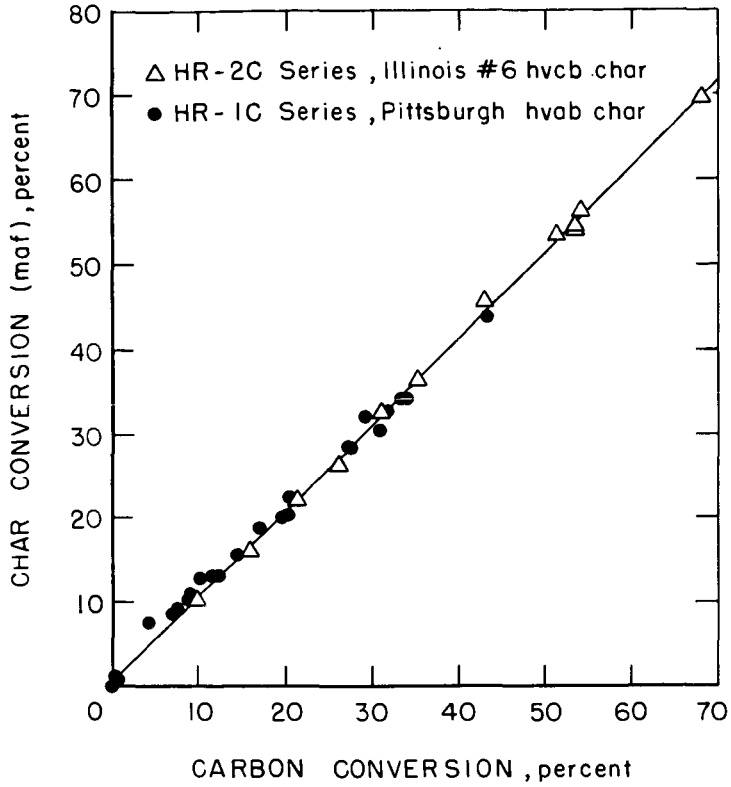


Figure 29- Char conversion (maf) as a function of carbon conversion during hydrogasification.

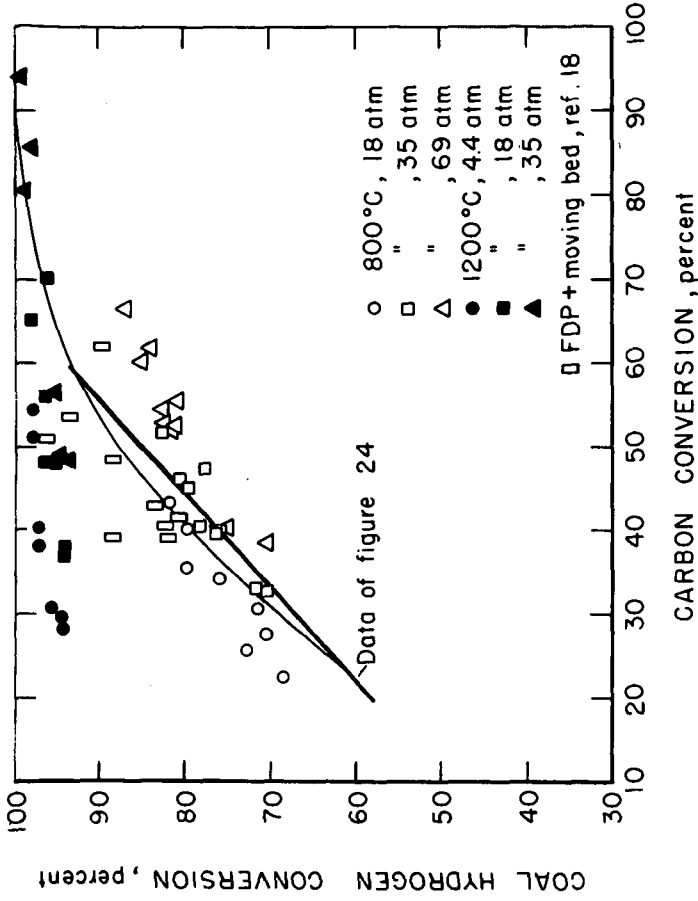


Figure 30-Conversion of coal hydrogen in HR-I tests.

5-20-75 L-14302

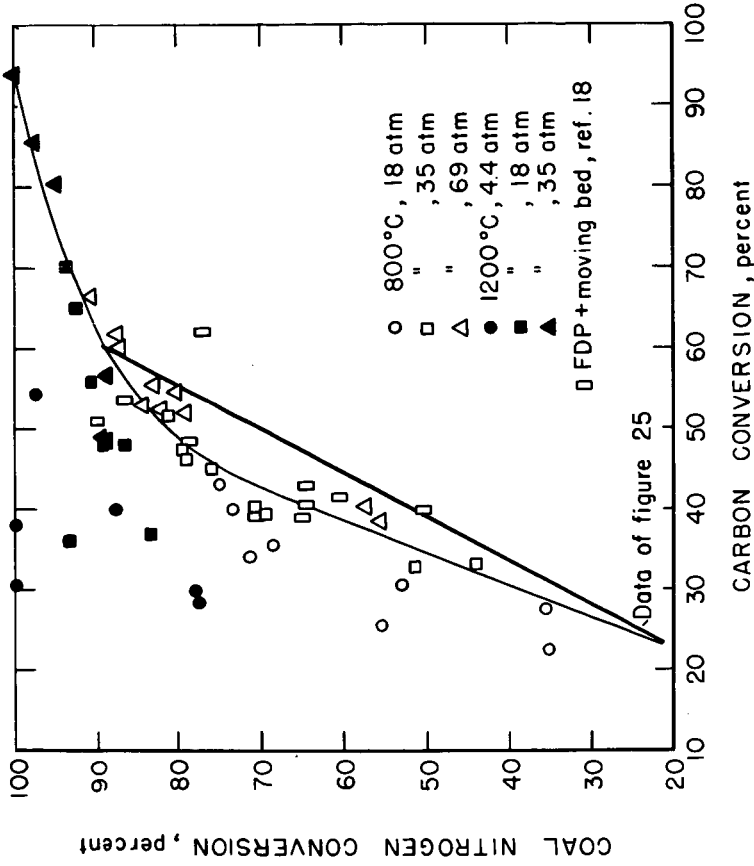


Figure 31- Conversion of coal nitrogen in HR-I tests

5-21-75

L-14303

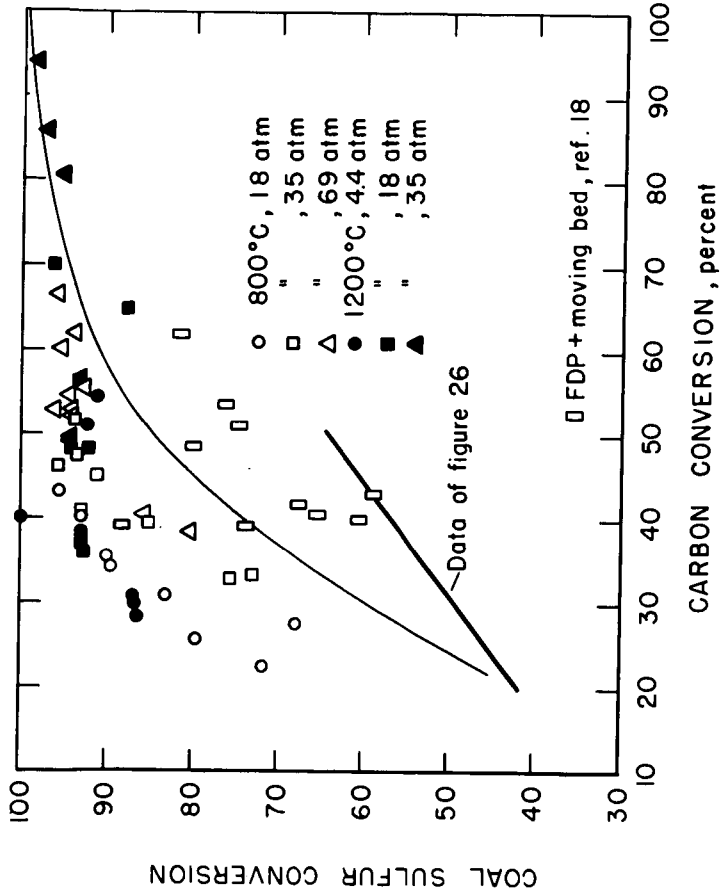
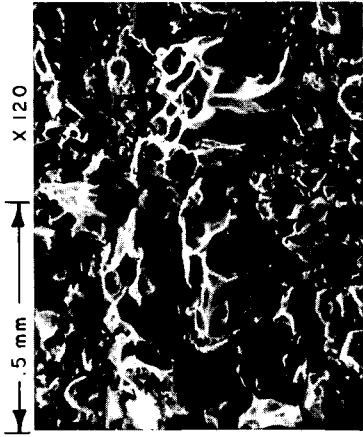


Figure 32 - Conversion of coal sulfur in HR-1 tests

5-20-75

L-14304



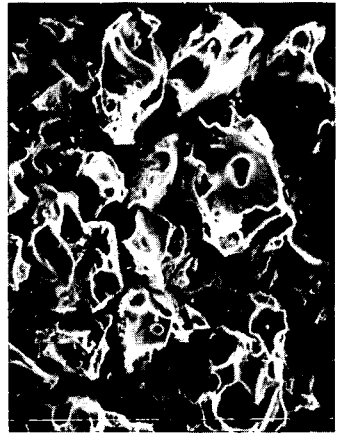
800°C- 2 min.



800°C- 10 min.



600°C- 2 min.

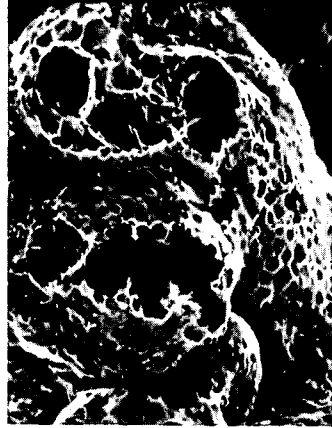


600°C- 10 min.

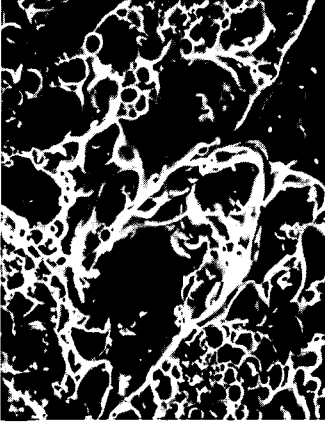
Figure 20 - SEM PHOTOGRAPHS OF 'HOT' ROD CHAR AT VARIOUS TEMPERATURES  
(69 atm) X 120



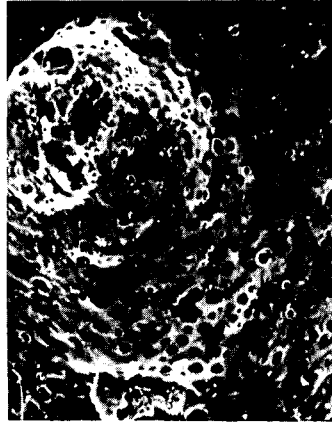
850°C- 137 atm



900°C- 35 atm



725°C- 205 atm



850°C- 69 atm

Figure 19 - SEM PHOTOGRAPHS OF FDP CHAR AT VARIOUS PRESSURES , X 120

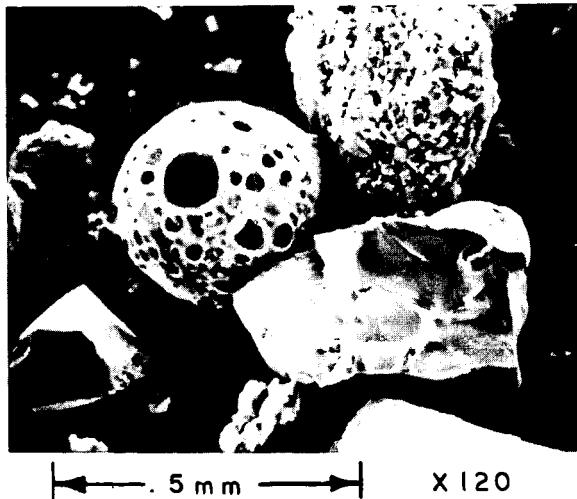
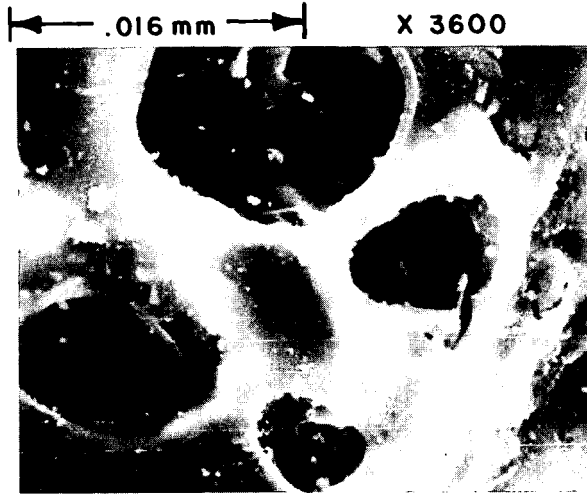


**Figure 21 - SEM PHOTOGRAPHS OF FDP CHAR (LIGNITE) ,  
(850°C, 69 atm)**